1998

Capacity Fade Mechanisms and Side Reactions in Lithium-Ion Batteries

Pankaj Arora
University of South Carolina - Columbia

Ralph E. White
University of South Carolina - Columbia, white@cec.sc.edu

Marc Doyle

Publication Info

Published in *Journal of the Electrochemical Society*, Volume 145, Issue 10, 1998, pages 3647-3667.

Capacity Fade Mechanisms and Side Reactions in Lithium-Ion Batteries

Pankaj Arora* and Ralph E. White**

Center For Electrochemical Engineering, Department of Chemical Engineering, University of South Carolina, Columbia, South Carolina 29208, USA

Marc Doyle**

DuPont Central Research and Development, Experimental Station, Wilmington, Delaware 19880-0262, USA

ABSTRACT

The capacity of a lithium-ion battery decreases during cycling. This capacity loss or fade occurs due to several different mechanisms which are due to or are associated with unwanted side reactions that occur in these batteries. These reactions occur during overcharge or overdischarge and cause electrolyte decomposition, passive film formation, active material dissolution, and other phenomena. These capacity loss mechanisms are not included in the present lithium-ion battery mathematical models available in the open literature. Consequently, these models cannot be used to predict cell performance during cycling and under abuse conditions. This article presents a review of the current literature on capacity fade mechanisms and attempts to describe the information needed and the directions that may be taken to include these mechanisms in advanced lithium-ion battery models.

Introduction

The typical lithium-ion cell[1-3] (Fig. 1) is made up of a coke or graphite negative electrode, an electrolyte which serves as an ionic path between electrodes and separates the two materials, and a metal oxide (such as $LiCoO_2$, $LiMn_2O_4$, or $LiNiO_2$) positive electrode. This secondary (rechargeable) lithium-ion cell has been commercialized only recently.[4-7] Batteries based on this concept have reached the consumer market, and lithium-ion electric vehicle batteries are under study in industry. The lithium-ion battery market has been in a period of tremendous growth ever since Sony introduced the first commercial cell in 1990.[8,9] With energy density exceeding 130 Wh/kg (e.g., Matsushita CGR 17500)[10] and cycle life of more than 1000 cycles (e.g., Sony 18650)[10] in many cases, the lithium-ion battery system has become increasingly popular in applications such as cellular phones, portable computers, and camcorders. As more lithium-ion battery manufacturers enter the market and new materials are developed, cost reduction should spur growth in new applications. Several manufacturers such as Sony Corporation, Sanyo Electric Company, Matsushita Electric Industrial Company, Moli Energy Limited, and A&T Battery Corporation have started manufacturing lithium-ion batteries for cellular phones and laptop computers. Yoda[11] has considered this advancement and described a future battery society in which the lithium-ion battery plays a dominant role.

Several mathematical models of these lithium-ion cells have been published.[12-35] Unfortunately, none of these models include capacity fade processes explicitly in their mathematical description of battery behavior. The objective of the present work is to review the current understanding of the mechanisms of capacity fade in lithium-ion batteries. Advances in modeling lithium-ion cells must result from improvements in the fundamental understanding of these processes and the collection of relevant experimental data.

Some of the processes that are known to lead to capacity fade in lithium-ion cells are lithium deposition (overcharge conditions), electrolyte decomposition, active material dissolution, phase changes in the insertion electrode materials, and passive film formation over the electrode and current collector surfaces. Quantifying these degradation processes will improve the predictive capability of battery models ultimately leading to less expensive and higher quality batteries. Significant improvements are required in performance standards such as energy density and cycle life, while maintaining high environmental, safety, and cost standards. Such progress will require considerable advances in our understanding of electrode and electrolyte materials, and the fundamental physical and chemical processes that lead to capacity loss and resistance increase in commercial lithium-ion batteries. The process of developing mathematical models for lithium-

* Electrochemical Society Student Member.
** Electrochemical Society Active Member.

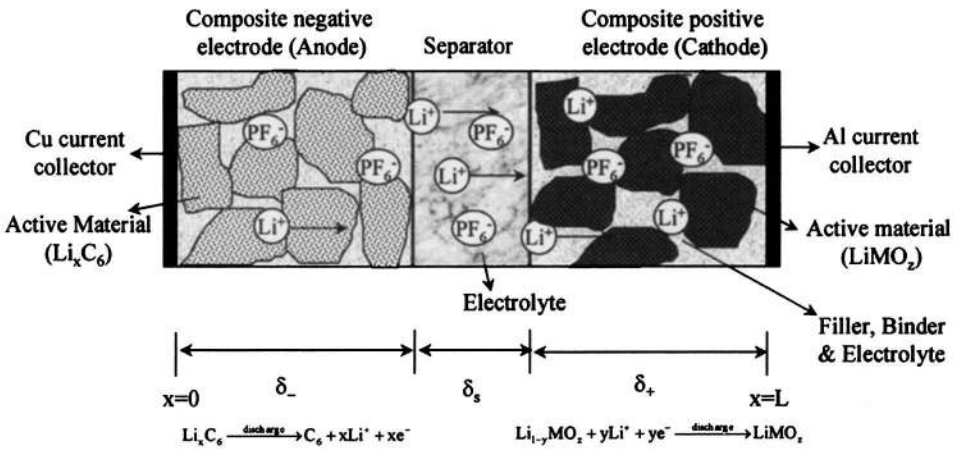

Fig. 1. Schematic diagram of a lithium-ion cell on discharge.

ion cells that contain these capacity fade processes not only provides a tool for battery design but also provides a means of understanding better how these processes occur.

Present Lithium-Ion Battery Models

The development of a detailed mathematical model is important to the design and optimization of lithium secondary cells and critical in their scale-up. West et al.[12-15] developed a pseudo two-dimensional model of a single porous insertion electrode accounting for transport in the solution phase for a binary electrolyte with constant physical properties and diffusion of lithium ions into the cylindrical electrode particles. The insertion process was assumed to be diffusion limited, and hence charge-transfer resistance at the interface between electrolyte and active material was neglected. Later Mao and White developed a similar model with the addition of a separator adjacent to the porous insertion electrode.[16] These models cover only a single porous electrode; thus, they do not have the advantages of a full-cell-sandwich model for the treatment of complex, interacting phenomena between the cell layers. These models confine themselves to treating insertion into TiS_2 with the kinetics for the insertion process assumed to be infinitely fast. Spotnitz et al.[17] accounted for electrode kinetics in their model for discharge of the TiS_2 intercalation cathode.

The galvanostatic charge and discharge of a lithium metal/solid polymer separator/insertion positive electrode cell was modeled using concentrated-solution theory by Doyle et al.[18,20] The model is general enough to include a wide range of separator materials, lithium salts, and composite insertion electrodes. Concentrated-solution theory is used to describe the transport processes, as it has been concluded that ion pairing and ion association are very important in solid polymer electrolytes.[36] This approach also provides advantages over dilute solution theory to account for volume changes. Butler-Volmer-type kinetic expressions were used in this model to account for the kinetics of the charge-transfer processes at each electrode. The positive electrode insertion process was described using Fick's law with a constant lithium diffusion coefficient in the active material. The volume changes in the system and film formation at the lithium/polymer interface were neglected and a very simplistic case of constant electrode film resistances was considered. Long-term degradation of the cell due to irreversible reactions (side reactions) or loss of interfacial contact is not predictable using this model.

Fuller et al.[19,21] developed a general model for lithium-ion insertion cells that can be applied to any pair of lithium-ion insertion electrodes and any binary electrolyte system given the requisite physical property data. Fuller et al.'s work demonstrated the importance of knowing the dependence of the open-circuit potential on the state of charge for the insertion materials used in lithium-ion cells. The slopes of these curves control the current distribution inside the porous electrodes, with more sloped open-circuit potential functions leading to more uniform current distributions and hence better utilization of active material. Optimization studies were carried out for the Bellcore plastic lithium-ion system.[37,38] The model was also used to predict the effects of relaxation time[19,39] on multiple charge-discharge cycles and on peak power.

Doyle et al.[22] modified the dual lithium-ion model to include film resistances on both electrodes and made direct comparisons with experimental cell data for the $Li_xC_6|LiPF_6$, ethylene carbonate/dimethyl carbonate (EC/DMC), Kynar FLEX®$|Li_yMn_2O_4$ system. Comparisons between data and the numerical simulations suggested that there is additional resistance present in the system not predicted by present models. The discharge performance of the cells was described satisfactorily by including either a film resistance on the electrode particles or by contact resistances between the cell layers or current-collector interfaces. One emphasis of this work was in the use of the battery model for the design and optimization of the cell for particular applications using simulated Ragone plots.

Thermal modeling is very important for lithium batteries because heat produced during discharge may cause either irreversible side reactions or melting of metallic lithium. Chen and Evans carried out a thermal analysis of lithium-ion batteries during charge-discharge and thermal runaway using an energy balance and a simplified description of the electrochemical behavior of the system.[25-27] Their analysis of heat transport and the existence of highly localized heat sources due to battery abuse indicated that localized heating may raise the battery temperature very quickly to the thermal runaway onset temperature, above which it may keep increasing rapidly due to exothermic side reactions triggered at high temperature. Pals and Newman developed a model to predict the thermal behavior of lithium metal-solid polymer electrolyte cells and cell stacks.[28,29] This model coupled an integrated energy balance to a full-cell-sandwich model of the electrochemical behavior of the cells. Both of these models emphasized the importance of considerations of heat removal and thermal control in lithium-polymer battery systems.

Verbrugge and Koch developed a mathematical model for lithium intercalation processes associated with a cylindrical carbon microfiber.[30,31] They characterized and modeled the lithium intercalation process in single-fiber carbon microelectrodes including transport processes in both phases and the kinetics of charge transfer at the interface. The primary purpose of the model was to predict the potential as a function of fractional occupancy of intercalated lithium. The overcharge protection for a Li/TiS_2 cell using redox additives has been theoretically analyzed in terms of a finite linear diffusion model by Narayanan et al.[32]

Darling and Newman modeled a porous intercalation cathode with two characteristic particle sizes.[33] They reported that electrodes with a particle size distribution show modestly inferior capacity-rate behavior and relaxation on open circuit is substantially faster when the particles are uniformly sized. Nagarajan et al.[34] modeled the effect of particle size distribution on the intercalation electrode behavior during discharge based on packing theory.[40] They observed that during pulse discharge, an electrode consisting of a binary mixture displays higher discharge capacity than an electrode consisting of single-sized particles. The current from the smaller particles reverses direction during the rest period which cannot be observed in the case of an electrode comprised of the same-sized particles. Recently Darling and Newman[35] made a first attempt to model side reactions in lithium batteries by incorporating a solvent oxidation side reaction into a lithium-ion battery model. Even though a simplified treatment of the oxidation reaction was used, their model was able to make several interesting conclusions about self-discharge processes in these cells and their impact on positive electrode state-of-charge.

A number of models having varying degrees of sophistication have been developed for lithium rechargeable batteries. For the most part, these models consider the ideal behavior of the systems, neglecting the phenomena that lead to losses in capacity and rate capability during repeated charge-discharge cycles. Fundamental models of these latter phenomena are less common because these processes are not as well understood. Also, models of failure modes in batteries do not usually have general applicability to a wide range of systems. However, the importance of these phenomena in the safe and efficient operation of high-energy lithium-ion batteries requires that they be incorporated into future battery models.

Capacity Fading Phenomenon

Side reactions and degradation processes in lithium-ion batteries may cause a number of undesirable effects leading to capacity loss. Johnson and White have shown that the capacities of commercial lithium-ion cells fade by ca. 10-40% during the first 450 cycles.[10] A flow chart describing many of the processes leading to capacity fade is shown

in Fig. 2. In Fig. 3, the capacity fade processes are shown on half-cell discharge curves. This gives a clearer picture of the processes by demonstrating where each is expected to manifest itself during operation of the battery. Below, we discuss each of these processes in some detail, after first discussing the general topic of capacity balance.

Capacity Balancing in Lithium-Ion Cells

Lithium-ion cells operate by cycling lithium ions between two insertion electrode hosts having different insertion energies. For optimum performance, the ratio of the lithium-ion capacities of the two host materials should be balanced. Capacity balancing refers to the optimization of the mass loading in the two electrodes to achieve the maximum capacity (or energy) from the battery under conditions of steady cycling. Due to the practical importance of this subject for maximizing cell performance, as well as the safety implications with poorly balanced cells, this subject has been discussed in the literature by several authors.[2,22,37,38]

The condition for balanced capacities in a lithium-ion cell can be written in terms of a ratio γ of active masses in the electrodes. Written as a ratio of positive to negative electrode masses, this expression is[20]

$$\gamma = \frac{m_+}{m_-} = \frac{\delta_+ \epsilon_+ \rho_+}{\delta_- \epsilon_- \rho_-} = \frac{\Delta x C_-}{\Delta y C_+} \quad [1]$$

This equation says that the desired mass ratio depends on the relative coulombic capacities of the two electrodes (C is in units of mAh/g) and the amount of cyclable lithium in each. The cyclable lithium is quantified in terms of the range of lithium stoichiometry in the insertion electrode that can be cycled reversibly, with the notation that Δx refers to the range of negative electrode stoichiometry and Δy to the positive electrode. For some insertion materials, which have several plateaus over which lithium can be inserted and deinserted, one may choose to cycle over only a limited range of stoichiometry for reversibility or safety reasons. In these cases, the stoichiometric range entered in the above formula would be reduced from its maximum value.

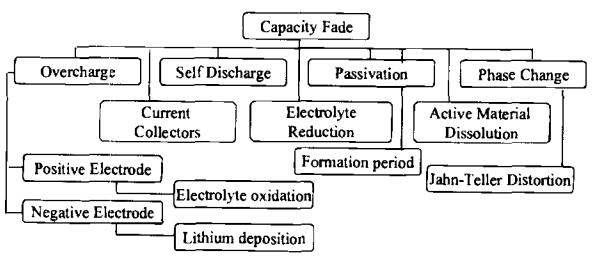

Fig. 2. Flow chart describing various capacity fade phenomena in lithium-ion batteries.

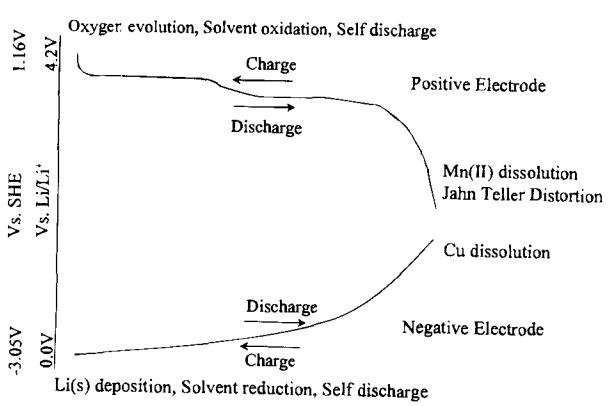

Fig. 3. Half-cell discharge curves showing various capacity fade phenomena.

For example, consider the case of a lithium-ion cell having a petroleum coke negative electrode and a lithium manganese oxide spinel positive electrode. By choice, we can assign useful ranges of stoichiometries for the two electrode materials of 0.61 for the coke and 0.83 for the lithium manganese oxide. These stoichiometric ranges correspond to the following electrochemical processes

$$C_6 + 0.61Li^+ + 0.61e^- \underset{\text{discharge}}{\overset{\text{charge}}{\rightleftharpoons}} Li_{0.61}C_6 \quad [2]$$

$$LiMn_2O_4 \underset{\text{discharge}}{\overset{\text{charge}}{\rightleftharpoons}} 0.83Li^+ + 0.83e^- + Li_{0.17}Mn_2O_4 \quad [3]$$

The active mass ratio needed to cycle these two materials in the manner shown here is equal to 1.85. This is calculated by using the theoretical capacities of both positive and negative electrode (C_+ = 148 mAh/g and C_- = 372 mAh/g), equal to F divided by the molecular weight of the electrode material in its discharged state.

The situation above describes an "ideal" lithium-ion cell in which the capacity balance does not change over the life of the cell. For an ideal cell, the initial lithium capacity available for cycling is constant over the life of the battery. Unfortunately, the true case in actual lithium-ion batteries is more complicated than this, and side reactions and secondary processes are able to perturb the capacity balance from its ideal state. The actual optimized active mass ratio is ca. 2.05-2.15 for the coke/$LiMn_2O_4$ system, which corresponds to 14% excess capacity in the positive electrode.[41] This excess capacity is a measure of the amount of lithium needed to form a stable film over the electrode surfaces. A major process that affects the capacity balance is the initial formation period needed to passivate carbon-based electrodes. It is now well known that carbonaceous lithium insertion electrodes have irreversible capacity associated with the initial charging cycles.[42-46] This irreversible capacity loss is thought to result in the formation of a lithium conducting solid electrolyte interface (SEI) layer on the surface of the carbon, while in the process consuming some portion of the cyclable lithium ions in the cell. The loss of cyclable lithium to create this passivation layer has a profound impact on the capacity balance in the cell because it can remove a significant portion of the cyclable lithium depending on the type of carbon used.

If the cyclable lithium in the cell is reduced due to side reactions of any type, the capacity balance is changed irreversibly and the degree of lithium insertion in both electrodes during cell cycling is changed. Consider the case of the initial carbon passivation process that occurs on all lithium-ion cells using carbon-based electrodes. The cell is assembled initially in the discharged state, with the carbon free of lithium and the metal oxide positive electrode at its maximum lithium content. The amount of lithium in either electrode can be represented as shown in Fig. 4, which illustrates the difference between the ideal and actual carbon/$LiMn_2O_4$ lithium-ion system during the first few cycles.

In an ideal lithium-ion cell (Fig. 4a), all of the lithium should be intercalated into the negative electrode from the positive electrode during the first charge. Similarly, all of the lithium ions should be intercalated back into the positive electrode during the first discharge. In an actual lithium-ion cell, upon charging the cell for the first time, some portion of the lithium removed from the $LiMn_2O_4$ positive electrode goes into the irreversible film formation reaction while the remainder inserts into the carbon structure. The capacity due to the irreversible reaction is represented schematically in Fig. 4b by the smaller box below the negative electrode. After the cell is finished charging to some arbitrary cutoff voltage, the positive electrode has been delithiated to the extent possible under the charging conditions and the negative electrode is as full of lithium as possible given the amount of positive electrode mass available. Ideally, the lithium content in the carbon at this

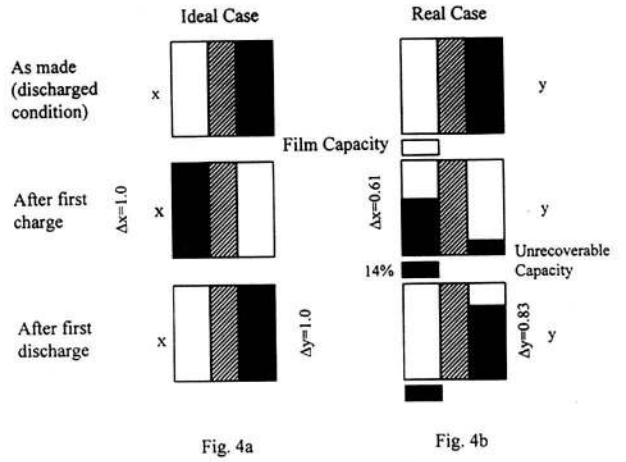

Fig. 4a Fig. 4b

Fig. 4. Schematic representation of loss of lithium-ion capacity to irreversible film formation in the coke/$LiMn_2O_4$ system.

point is at its maximum safe value. Also, we can imagine that the passivation layer is fully formed on the initial charging cycle, having consumed a certain amount of cyclable lithium irreversibly.

When this cell is now discharged for the first time, the total quantity of lithium available for discharge is equal only to the amount of lithium reversibly inserted into the carbon electrode. Hence, the initial irreversible lithium lost cannot be recovered or utilized. The discharge proceeds until all of the reversible lithium is removed from the carbon electrode. At this time, the stoichiometry in the positive electrode will not reach its initial value upon cell assembly due to the capacity lost on the initial charging cycle. This situation is reflected in Fig. 4 in the bottom diagram. If the cell operates without any additional side reactions for the rest of its life, it will still never utilize the full range of stoichiometry available in the positive electrode. Thus for the above carbon/$LiMn_2O_4$ system it is safe to cycle within the limits of $\Delta x = 0.61$ (x varying from 0 to 0.61) and $\Delta y = 0.83$ (y varying from 0.17 to 1.0) as shown in Fig. 4. It should be remembered that these Δx and Δy values are cell and material specific.

The range of stoichiometries accessed in the negative electrode in this example depends on the positive to negative mass ratio parameter γ. If the ideal value of γ had been used to fabricate this example cell, the initial loss of lithium due to the irreversible passivation process would prevent the carbon electrode from being fully utilized to an extent that depended directly on the amount of irreversible capacity that the particular carbon electrode material exhibited. Rather than let this happen, the common procedure is to assemble cells having a greater than theoretical amount of positive-electrode mass, thus allowing for losses of cyclable lithium during operation by initially providing extra lithium. One method of providing the extra lithium without increasing the cathode mass is to use overlithiated manganese oxide ($Li_{1+x}Mn_2O_4$) spinel electrodes as proposed by Tarascon et al.[47,48] and Peramunage et al.[49]

Even with side reactions and irreversible capacity losses, the desired mass ratio can still be calculated via a formula analogous to the above one, although we must now include in the negative electrode capacity an additive contribution due to the passivation process. Referring to this contribution as C_{irr} (mAh/g), the capacity balancing condition can be expressed as

$$\gamma = \frac{\Delta x C_- + C_{irr}}{\Delta y C_+} \quad [4]$$

For example, in the case of a lithium-ion cell fabricated using a carbon (petroleum coke) negative electrode and a lithium manganese oxide spinel positive electrode, the actual mass ratio desired for optimum utilization of the two electrodes is about 14% larger than its theoretical value. This excess capacity is a measure of the amount of lithium needed to form a stable film over the electrode surfaces. The active mass ratio for the graphite/$LiMn_2O_4$ system is ca. 2.4-2.45.[37] Smaller mass ratios will prevent full utilization of the negative electrode whereas larger mass ratios present a safety hazard because the negative electrode can be overcharged (more lithium is available to insert into the electrode than is desirable). Overall cell performance such as energy density is maximized at the optimum mass ratio only.

It should also be apparent that there is a relationship between the expected overcharge and overdischarge processes and the cell's capacity balance. For example, in the case of the lithium manganese oxide spinel material discussed above, overcharge reactions involving solvent oxidation depend on the capability of the cell to fully oxidize the positive electrode during normal cycling conditions. For cells with high mass ratios, this may not be possible because the negative electrode becomes fully charged before allowing the positive to become fully charged (i.e., before complete removal of lithium from the positive). Overdischarge of high-mass-ratio cells will affect the negative electrode by emptying the carbon of lithium completely and then driving the negative electrode potential up to an undesirably high value. In other cases, the mass ratio may be lower than desired leading to overcharge of the positive electrode. For example, in the case of the coke/$LiMn_2O_4$ system, mass ratios higher than 2.1 can lead to overlithiation of the negative electrode during charge. Mass ratios lower than 2.1 will have less lithium available than needed and will thus result in overdischarge of the negative electrode with accompanying negative safety or performance consequences.

The carbon passivation process is the most common and well-studied example of a side reaction in the lithium-ion cell that will change the capacity balance.[50,51] However, a number of other processes are also capable of having this effect. Any side reaction that either produces or consumes lithium ions or electrons will lead to a change in the cell's capacity balance, with the potential to impact negatively the cell's performance. In addition, once the capacity balance is changed from its desired state, the changes are generally irreversible and may accumulate over many cycles to generate a hazardous condition in the cell. Although difficult to quantify experimentally, it is straightforward to follow these effects using battery models and computer simulations under dynamic conditions if the relevant phenomena are included in the models.

Formation Cycles

Lithium-ion cells exhibit a sharp decay in capacity during the first few cycles. This period is known as the formation period during which cells are conditioned prior to use. It is generally desirable for the capacity decay observed after the formation period to be very small compared to the total cell capacity, after which the charge-discharge reactions are nearly 100% efficient. The sharp decay in capacity is due primarily to the solid electrolyte interface layer formation on the negative electrode. Passivation of the carbon electrode during the formation period and subsequent capacity loss are highly dependent on specific properties of the carbon in use, such as degree of crystallinity, surface area, pretreatments, and other synthesis and process details.[42,44-46,52] After the first few cycles, the cell stabilizes and exhibits a constant capacity. The formation cycles are one of the critical steps in the manufacture of lithium-ion systems. For graphitic materials such as Osaka Gas mesocarbon micobeads (MCMB), the irreversible capacity is as low as 8 to 15%, whereas for hard carbons it can be as high as 50% of the reversible capacity.

Fong et al.[42] demonstrated that irreversible reactions occur on carbon-based electrodes during the first discharge in carbonate-based electrolytes prior to the reversible insertion-deinsertion of lithium ions. These irreversible reactions are associated with electrolyte decomposition and cause the formation of a passivating film or solid electrolyte interface

on the surface of the carbon. When all the available surface area is coated with a film of decomposition products, further reaction stops. In subsequent cycles, these cells exhibit excellent reversibility and can be cycled without capacity loss for many cycles. These authors first showed that the reversible insertion of lithium into graphitic carbons was possible as long as the proper passivating solvent was present. Gas evolution was observed by Gozdz et al.[53] during the formation of the passivation layer on the carbon electrode during the first charge of a lithium-ion cell. The gas evolved correlated well with the irreversible capacity loss observed during the formation cycle. More details of carbon passivation in various solvent systems and the mechanisms of the passivation process are reviewed in later sections on electrolyte reduction and film formation.

The formation period is critical in lithium-ion battery manufacture because of its economic impact. First, it obligates manufacturers to invest in battery cycling stations to cycle cells several times before sending them to market, consuming both time and resources. Second, irreversible capacity consumed during the formation period is lost to the battery, directly subtracting from the system's energy. Last, the formation period generates gases which under some conditions may need to be vented prior to further operation of the cell. Research efforts worldwide continue to generate very high capacity carbon electrode materials having high irreversible capacities. To utilize these materials in the most efficient manner requires a prepassivation or prelithiation scheme not involving the sacrifice of a substantial quantity of the cyclable lithium available in the positive electrode. Although several research groups have been studying these processes and potential alternative approaches, there is no known solution for eliminating the formation period in an economically feasible manner.

Overcharge Phenomena

Under conditions of overcharge, major capacity losses have been observed in all types of lithium-ion cells. The poor overcharge resistance of commercial lithium-ion cells and the safety issues that result from overcharge have led to tight control over charging and discharging of commercial cells using built-in electronic circuitry. The future application of lithium-ion cells in new areas would be facilitated by advances in understanding and controlling overcharge. In particular, the use of lithium-ion cells in multicell bipolar stacks requires a greater degree of overcharge tolerance due to the difficulty in achieving uniform utilization of all cells in series stacks.

Overcharge losses can be classified into three main types at present: (*i*) overcharge of coke and graphite-based negative electrodes, (*ii*) overcharge reactions for high-voltage positive electrodes, and (*iii*) overcharge/high-voltage electrolyte oxidation processes. These side reactions lead to loss of the active material and consumption of electrolyte, both of which can lead to capacity loss in the cell.

Overcharge of Coke and Graphite-Based Negative Electrodes

During overcharge of lithium-ion cells, metallic lithium may be deposited on the negative electrode surface as the primary side reaction. This reaction is expected for cells with excess cyclable lithium due to either higher than desired initial mass ratio or lower than expected lithium losses during the formation period. The freshly deposited lithium covers the active surface area of the negative electrode leading to a loss of the cyclable lithium and consumption of electrolyte because of the highly reactive nature of metallic lithium. This phenomenon may occur at high charge rates even for cells with the correct mass ratio because of the polarization at the negative electrode under these conditions.[22] However, the more common circumstance leading to lithium deposition is poorly balanced cells having too much positive electrode mass initially. The primary side reaction involved in the overcharge process is

$$Li^+ + e^- \rightarrow Li(s) \qquad [5]$$

and the intercalation-deintercalation reaction on the negative electrode (coke or graphite) may be written

$$C_6 + xLi^+ + xe^- \underset{\text{discharge}}{\overset{\text{charge}}{\rightleftharpoons}} Li_xC_6 \qquad [6]$$

Lithium metal deposited on the negative electrode reacts quickly with the solvent or salt molecules in the vicinity giving Li_2CO_3, LiF, or other products.[42,54] The lithium metal is expected to form near the electrode-separator boundary where the electrode potential is more negative. The products formed may block the pores, leading to a loss of rate capability as well as capacity losses. Formation of lithium metal is also a safety hazard due to its extreme reactivity with the liquid solvents. Lithium metal deposition may be more of a concern with graphitic carbon electrodes than with coke electrodes due to the lower average open-circuit potential of the former. For this reason, mass ratios in cells using graphite are usually chosen to be smaller than the optimum in order to provide a buffer against lithium deposition, with the negative consequence that the full 372 mAh/g capacity of the graphite is not attained.

Overcharge Reactions for High-Voltage Positive Electrodes

Overcharging the positive electrodes in lithium-ion cells can lead to a wide variety of electrochemical reactions depending on the details of the system chemistry. As with the negative electrode, the extent to which overcharging is expected at the positive electrode depends on the system's capacity balance. For cells with too low a mass ratio, the positive electrode is stressed to a greater extent during charging and overcharge becomes a possibility. Overcharging the positive electrode can lead to capacity loss due to inert material formation (e.g., Co_3O_4) or solvent oxidation due to the high positive electrode potential. Formation of electrochemically inactive electrode decomposition products leads to a capacity imbalance between the electrodes. Thermal abuse of the positive electrode can lead to oxygen loss from the metal oxide lattice. This oxygen can increase the pressure inside the cell and represents a potential safety concern.

Dahn et al.[52] proposed the following decomposition reactions for the three main positive electrode materials in their charged states under abuse conditions. The reaction proposed for $LiCoO_2$ can be expressed as

$$Li_yCoO_2 \rightarrow \frac{(1-y)}{3}[Co_3O_4 + O_2(g)] + yLiCoO_2, \quad \text{where } y < 0.4 \qquad [7]$$

for $LiNiO_2$[52]

$$Li_{y<0.3}NiO_2 \rightarrow LiNi_2O_4 + O_2(g) \qquad [8]$$

and for γ-MnO_2[52] as

$$\lambda - MnO_2 \rightarrow \frac{1}{2}Mn_2O_3 + \frac{1}{4}O_2(g) \qquad [9]$$

They observed that λ-MnO_2 is more tolerant toward electrical and thermal abuse than Li_yNiO_2 and Li_yCoO_2. Oxygen loss from the metal oxides was observed when $y < 1$ and increased with decreasing stoichiometry. This loss of oxygen began at 200°C for $Li_{0.3}NiO_2$, 240°C for $Li_{0.4}CoO_2$, and about 385°C for λ-MnO_2, when heated at a rate of 1°C/min. The higher the heating rate, the higher is the O_2 onset temperature and vice versa. Formation of oxygen in the sealed cell in the absence of any recombination mechanism (as exists in Ni-Cd, Pb-acid, and Ni-MH cells using aqueous electrolytes) is a safety concern because of the accumulation of flammable gas mixtures in the cell. Also, the final metal oxide products such as Co_3O_4, $LiNi_2O_4$, and Mn_2O_3 are inert to lithium insertion-deinsertion, and hence capacity is lost irreversibly.

Staniewicz[55] proposed an overcharge mechanism for their $LiNiO_2$ electrodes by accounting for all the lithium

ions in $LiNiO_2$-based cells. They divided the cycling process for the $LiNiO_2$ electrode into three phases.

Phase I.—Lithium ions used to passivate carbon irreversibly and/or not able to cycle back into the $LiNiO_2$

$$LiNiO_2 \rightarrow 0.15Li^+ + Li_{0.85}NiO_2 + 0.15e^- \quad [10]$$

Phase II.—Reversible cycling

$$Li_{0.85}NiO_2 \rightarrow 0.5Li^+ + Li_{0.35}NiO_2 + 0.5e^- \quad [11]$$

Phase III.—Overcharge

$$Li_{0.35}NiO_2 \rightarrow 0.35Li^+ + NiO_2 + 0.35e^- \quad [12]$$

The first phase accounts for the lithium ions used to form the passive film, the second phase for reversible cycling, and the third phase accounts for the lithium ions removed during overcharge. The overcharge reaction proposed by Staniewicz[55] does not agree with the mechanism proposed by Dahn et al.[52] for Li_yNiO_2 electrodes under conditions of thermal abuse. Moreover, NiO_2 is not usually thought to be stable due to the Ni(IV) oxidation state.[56] No experimental data were provided by the author to support the above hypotheses.

The formation of low lithium content Li_yNiO_2 ($y < 0.2$) has been stated as a cause of cell failure during cycling.[57] In addition, the material becomes highly catalytic toward electrolyte oxidation, and some of the nickel ions may migrate to lithium sites. The first cycle irreversibility is primarily related to the amount of Ni^{II} between the slabs of NiO_2, which requires extra charge for oxidation to a higher valence state. The stability of the structure of $LiNiO_2$ at low lithium content can be improved by substituting Ni with Al or B.[57]

Recently, the thermal stability of $LiNiO_2$ cathodes has been studied in detail by substituting a portion of the Ni or Li with other elements (Co, Mn, Mg, Ca, Sr, Ba).[58-61] The substitution of Ni with Co improves the cycling behavior at room temperature, but the cycling characteristics at high temperatures remain unsatisfactory.[60,61] Substituting a part of the Ni in $LiNiO_2$ with alkaline earth metals (Mg, Ca, Sr, Ba) and with Al improves the high-temperature and high-rate performance of these electrodes.[58] At high temperatures, the deterioration in the performance during charging and discharging is greatly influenced by a change in the chemical reactivity of the active material. In the presence of other substituents in the crystal structure, the reactivity decreases during deep charging and discharging and at high temperatures, which leads to a more stable material. In the case of $LiCoO_2$, the high-temperature performance is deteriorated by the introduction of other elements. When the Ni in $LiNiO_2$ is substituted with Ca, Nb, or In, the structural changes observed during the charging process are very small, which leads to better cyclability of these doped materials.[61]

The thermal stability of lithium manganese oxide spinel phases was studied by Thackeray et al.[62] They proposed that Li_2MnO_3 is formed and oxygen is evolved when the spinel is heated in the temperature range of 780 to 915°C. The rate of oxygen evolution increased above 915°C, and around 1200°C, both O_2 and Li_2O were lost. The above reactions are not electrochemical reactions and occur when the active material is heated to a particular temperature. Including thermally induced electrode decomposition reactions in a phenomenological battery model may not be necessary because battery failure will likely have occurred already at lower temperatures.

Gao and Dahn showed a correlation between the capacity fade of the spinel and the growth of the 3.3 V discharge plateau upon cycling.[63] The 3.3 V discharge plateau increased each time the cell was charged to a higher voltage, suggesting that $LiMn_2O_4$ tends to lose O_2 when overcharged. The following mechanism was proposed

$$El \rightarrow (Oxid\ El)^+ + e^- \quad [13]$$

and

$$LiMn_2O_4 + 2\delta e^- \rightarrow LiMn_2O_{4-\delta} + \delta O^{2-} \quad [14]$$

where El is the electrolyte solvent molecule and $(oxid\ El)^+$ denotes a positively charged electrolyte solvent molecule (radical cation). The radical cation $(oxid\ El)^+$ can be assumed to be very unstable and will participate in further side reactions immediately upon formation. One possible process would be dimerization of the radical with accompanying expulsion of two protons. If this cationic species is sufficiently stable to reach the negative electrode, it would undergo reduction either back to the original solvent species or to other products. Highly delocalized salt anions such as PF_6^- may help to stabilize cationic species such as these.

These authors state that the electrolyte may act as an electron donor to the partially delithiated spinel, inducing the oxygen loss from the oxide structure. It is possible that a second phase (similar to what is formed during heating) with the rock-salt structure forms at the surface of $LiMn_2O_4$ when it loses oxygen over the course of cycling. The loss of oxygen from the sample during cycling is undesirable, not only because it could induce structural damage to the sample surface impacting the cycling ability, but also because it tends to oxidize the electrolyte which also reduces the cell's life.

Overcharge/High Voltage Electrolyte Oxidation Processes

The electrolytes used in lithium-ion cells are mixtures of organic solvents and one or more lithium salts. The most popular electrolytes currently being used include mixtures of the linear and cyclic carbonates such as propylene carbonate (PC), ethylene carbonate (EC), dimethyl carbonate (DMC), diethyl carbonate (DEC), and ethyl methyl carbonate (EMC) and salts such as $LiPF_6$, $LiBF_4$, $LiAsF_6$, and $LiClO_4$. Sony reportedly uses a mixture of PC, DMC, and EMC with $LiPF_6$ salt, whereas Sanyo and Matsushita use mixtures of EC, DMC, and DEC and EC, DMC, DEC, and EMC, respectively, with $LiPF_6$.[10]

High voltage positive electrodes used in lithium-ion batteries present a stringent requirement for electrolyte stability and purity. The electrolyte choice is a limiting factor in lithium-ion batteries because the maximum voltage of the cell is limited by the decomposition potential of the electrolyte. Common electrolytes in use today decompose at high voltages (>4.5 V) forming insoluble products (Li_2CO_3, etc.)[42,54] which block the pores of the electrodes and cause gas generation in the cell. These effects can cause both capacity loss upon further cycling of the cell and can also be an extreme safety hazard. One particular solvent combination, EC/DMC, is in use in many systems alone and in combination with other solvents and is claimed to have the highest oxidation resistance among the common carbonate mixtures.[64] Campbell et al.[65] reported that the oxidation potential of pure PC is higher than that of PC containing electrolyte salts. This suggests that the electrochemical oxidation of nonaqueous electrolytes is enhanced by the presence of electrolyte salts.

Decomposition potentials are assessed experimentally by performing cyclic voltammetry either on inert metal surfaces or on actual insertion electrode materials and setting an arbitrary criterion on the current density above which solvent breakdown is assumed to be occurring. For irreversible electrochemical side reactions such as these, no thermodynamic open-circuit potential exists, and hence the decomposition potential does not have a firm meaning. Instead, these side reactions may often be described with Tafel equations which lead to a finite rate of decomposition at all voltages, increasing exponentially with increasing voltage.[35]

The decomposition potentials of many electrolytes are reported in Table I; however, it is not always clear whether the solvent or the salt or both are involved in the oxidation processes.[64,66-68] In addition, the ambiguity in reporting

values for solvent oxidation potentials is not always appreciated. These data are only well defined if the value of the current density at which the decomposition potential is assessed is given as well as the voltage scan rate and the electrode material used. We have taken the cyclic voltammetry data of Kanamura et al.[66] measured at a sweep rate of 50 mV/s and used the criterion of 0.1 mA/cm^2 as the threshold current density to define the oxidation potentials given in Table I. Data of Tarascon et al.[64] were used as given in their paper because the actual cyclic voltammagrams were not provided by these authors. Christie and Vincent[67] measured the oxidation potential using cyclic voltammetry at a sweep rate of 200 mV/s and used the criterion of 1 mA/cm^2. Ossolo et al.[68] used linear sweep voltammetry at a scan rate of 2 mV/s to determine the oxidation potential (E_{ox}) of various electrolytes on $Li_{1+x}V_3O_8$ electrodes. They assumed E_{ox} to be the potential at which a current density of 0.5 mA/cm^2 was recorded.

The solvent oxidation process can be stated in general as follows

solvent → oxidized products (gases, solution, and

solid species) + ne^- [15]

Any solvent (for example, PC or EC) oxidized will be lost, eventually leading to an increase in the salt concentration and a drop in the electrolyte level which will adversely affect the cell capacity. Also, the solvent oxidation products such as gases or other species will build up in the cell and cause a variety of problems. The rate of solvent oxidation depends on the surface area of the positive electrode material, current collectors, and the carbon black additive. In fact, the choice of carbon black and its surface area are critical variables because solvent oxidation may occur more on the carbon black than on the metal oxide electrode due to the higher surface area of the former.[38]

If a small part of the electrolyte is consumed during each charge, more electrolyte needs to be used when the cell is assembled. This implies less active material for a constant-volume container and consequently less initial capacity. Also, the solid products may form passivating layers on the electrodes that increase the polarization of the cell and thereby lower the output voltage of the battery.

Novak et al.[69] found that PC oxidizes at potentials as low as 2.1 V vs. Li/Li$^+$ on Pt and that the rate of oxidation increases substantially above 3.5 V. Depending on the electrode material, PC oxidation can begin at potentials as low as 2 V vs. Li/Li$^+$; however, a much greater degree of stability (up to and exceeding 4.5 V) is often exhibited by PC in practice. Cattaneo and Ruch[70] analyzed the volatile gaseous products from the decomposition of $LiClO_4$/PC and $LiAsF_6$/PC on heat-treated MnO_2 electrodes using on-line mass spectroscopy. Bulk oxidation of the electrolyte takes place above 4.0 V vs. Li/Li$^+$. CO_2 evolution was observed at low potentials (3.15 and 3.4 V vs. Li/Li$^+$) depending on the state of charge of the electrodes. No CO_2 was observed in the reverse (cathodic) scan.

Chlorinated species were formed from the decomposition of ClO_4^- ions above 4.5 V.[70] The species identified were ClO_2 and HCl, which were assumed to be formed by the following mechanism

$$ClO_4^- \rightarrow e^- + ClO_4 \rightarrow ClO_2 + 2\ O_{ad} + e^- \quad [16]$$

$$ClO_2 + H^+ + e^- \rightarrow HCl + O_2(g) \quad [17]$$

$$2\ O_{ad} \rightarrow O_2(g) \quad [18]$$

Eggert and Heitbaum[71] also observed the oxidation of perchlorate anions on a Pt electrode at potentials above 4.6 V vs. Li/Li$^+$ using differential electrochemical mass spectrometry (DEMS). The instability of ClO_2 in the presence of protons from the oxidation of PC will produce HCl. Oxygen evolution is also observed in the decomposition of $LiClO_4$ electrolytes.

Christie and Vincent[67] reported the oxidation potential for 1 M $LiPF_6$ in PC at a Ni microelectrode. Kanamura et al.[72,73] studied the ring opening of PC on Pt, Al, Au, and Ni electrodes. The PC oxidation potentials on these materials varied from 4.5 V for Ni to 6 V for Cu vs. Li/Li$^+$. It was shown by Kanamura et al.[73] that the anodic behavior of Ni electrodes in various propylene carbonate electrolytes depends strongly on the type of electrolyte salt used. The occurrence of decomposition products depends on the type of anion in the high electrode potential range. Electrolyte oxidation during overcharge of lithium-ion cells has been verified experimentally by Tarascon et al.[37] by cyclic voltammetry experiments. However, none of these studies provided mechanisms for the decomposition processes or used analytical techniques to study the products formed. Considering the large number of studies on solvent reduction in lithium batteries, and the relative importance of solvent oxidation to cell performance and safety, the lack of fundamental knowledge in this area is surprising.

Table I. Electrolyte oxidation potential of various electrolytes on different substrates.

Electrolyte	E_{ox} (V vs. Li/Li$^+$)	Substrate	Ref.
$LiClO_4$ + PC/DME (1:1)	4.6	LiV_3O_8	68
1 M $LiClO_4$ + PC	4.5	Ni	66
1 M $LiClO_4$ + PC	5.75	Al	66
1 M $LiClO_4$ + PC	5.2	Pt	66
1 M $LiClO_4$ + PC	5.5	Au	66
1 M $LiClO_4$ + EC/DEE (1:1)	4.55	$LiMn_2O_4$ + 10% carbon black	64
1 M $LiClO_4$ + EC/DMC (1:1)	>5.1	$LiMn_2O_4$ + 10% carbon black	64
$LiN(CF_3SO_2)_2$ + EC/DEE (1:1)	4.4	$LiMn_2O_4$ + 10% carbon black	64
$LiN(CF_3SO_2)_2$ + EC/DME (1:1)	4.35	$LiMn_2O_4$ + 10% carbon black	64
$LiCF_3SO_3$ + EC/DEE (1:1)	4.1	$LiMn_2O_4$ + 10% carbon black	64
$LiCF_3SO_3$ + EC/DMC (1:1)	3.2	$LiMn_2O_4$ + 10% carbon black	64
$LiBF_4$ + EC/DEE (1:1)	3.4	$LiMn_2O_4$ + 10% carbon black	64
$LiBF_4$ + EC/DMC (1:1)	>5.1	$LiMn_2O_4$ + 10% carbon black	64
$LiAsF_6$ + PC/DME (1:1)	4.7	LiV_3O_8	68
$LiAsF_6$ + PC	5.6	Pt	67
$LiAsF_6$ + PC/DME (1:1)	4.7	Pt	67
$LiAsF_6$ + EC/DMC (1:1)	4.7	$LiMn_2O_4$ + 10% carbon black	64
$LiAsF_6$ + EC/DEE (1:1)	3.9	$LiMn_2O_4$ + 10% carbon black	64
$LiPF_6$ + EC/DEE (1:1)	3.8	$LiMn_2O_4$ + 10% carbon black	64
$LiPF_6$ + EC/DMC (1:1)	>5.1	$LiMn_2O_4$ + 10% carbon black	64
$LiPF_6$ + PC	5.0	Ni	66, 67
$LiPF_6$ + PC	>5.1	$LiMn_2O_4$ + 10% carbon black	64
$LiPF_6$ + PC/EC (1:1)	>5.1	$LiMn_2O_4$ + 10% carbon black	64
$LiPF_6$ + DMC	>5.1	$LiMn_2O_4$ + 10% carbon black	64
$LiPF_6$ + DEC	3.8	$LiMn_2O_4$ + 10% carbon black	64
$LiPF_6$ + PC/DMC (1:1)	>5.1	$LiMn_2O_4$ + 10% carbon black	64
$LiPF_6$ + EC/DEC (1:1)	>4.8	$LiMn_2O_4$ + 10% carbon black	64

A detailed discussion of electrolyte decomposition (reduction) mechanisms is given in a later section.

Overcharge Protection[74-76]

Successful commercialization of lithium-ion batteries depends very much on their safety during operation under normal and especially under abusive conditions. An abuse condition generally leads to an increase in cell temperature which can initiate self-heating of the cell and eventually lead to thermal runaway.

The organic solvents commonly used to prepare electrolytes for lithium-ion batteries undergo irreversible oxidation at the positive electrode, which deleteriously affects the cycling performance of lithium batteries. A common way to avoid this is by including an additive in the electrolyte, an internal "chemical shuttle," to provide a current bypass mechanism when the cell exceeds a certain voltage.[75,76] The ideal chemical shuttle operates at or near the voltage of the fully charged cell and takes up the extra charge passed during overcharge, thereby preventing damaging reactions from proceeding. For typical lithium-ion cells, the desired potential of the redox process is approximately 4.5 to 5.0 V vs. Li/Li^+ or 1.5 to 1.0 V vs. H^+/H_2. In such a case, the electrochemical reactions sustained during overcharge at the positive and negative electrodes are[32,77]

$$R \rightarrow O + ne^- \quad [19]$$

$$O + ne^- \rightarrow R \quad [20]$$

Species O is generated at the positive electrode and diffuses to the negative electrode where it is reduced to R. The redox couple shuttles between the two electrodes to take up the excess charge input during overcharge and continues until charging is terminated.

For example, LiI functions as a good redox additive for overcharge protection at voltages close to the charged cell potential for certain 3 V lithium cells.[78-81] Its use in 1 M $LiPF_6$/THF solutions has been shown to avoid the oxidation of the electrolyte on Pt surfaces during overcharge. At anodic potentials (less positive than the fully charged cell potential), LiI undergoes a two-step process of oxidation of iodide ion to triiodide ion (3.2 V vs. Li/Li^+) and further oxidation of triiodide ion to iodine (3.65 V)

$$LiI \rightarrow I^- + Li^+ \quad [21]$$

$$3I^- \rightarrow I_3^- + 2e^- \quad [22]$$

$$2I_3^- \rightarrow 3I_2 + 2e^- \quad [23]$$

The iodine generated by the oxidation of LiI reacts chemically with lithium metal to regenerate LiI. The reduction of iodine occurs via a similar stepwise process of reduction of iodine to triiodide ion (3.55 V) and triiodide ion to iodide ion (2.75 V).

In addition to chemical shuttles, other methods of overcharge protection which are being used in commercial cells are

1. Separators with melting points of about 140°C can help in overcharge protection.[82,83] The purpose is to have a polymer membrane that melts and shuts off the current when the cell temperature rises above a given value during short-circuit conditions. The cells are prevented from reaching a high internal temperature by ceasing the reactions (and hence heat generation) when current is prevented from flowing across the separator. A number of polyolefin [e.g., polyethylene (130°C), and polypropylene (155°C)] based separators that can be used as internal safety devices by closing down the pores during short-circuit conditions have been developed.[84-87] Sony uses a polypropylene-based separator (161.7°C mp), whereas Sanyo and Matsushita use polyethylene-based separators with melting points of 135.4 and 133.4°C, respectively.[10] The shutdown temperature for Celgard® 2300 FSM is 131°C.[88]

2. Additives to the cathode mix, such as Li_2CO_3,[82] will decompose during overcharge and increase the pressure inside the cell. This pressure activates the vent present at the top of the cell, and the pressure is released and the circuit broken. The presence of excess additives does not greatly affect the current flow during normal operation of the cell, as shown in the Sony cell.[82] Moli Energy[89] has used 2 wt % biphenyl in their graphite/$LiCoO_2$ cells for overcharge protection. Solid biphenyl decomposition products deposit on the cathode resulting in high internal impedance and low rate capability.

3. Explosion-proof valves[74,82] become deformed upon increase of internal pressure of the cell to cut a connection lead contained in the cell. The supply of charging current is cut off when the pressure increases abnormally.

Electrolyte Decomposition (Reduction) Processes

Electrolyte reduction[41,47,48,64,90] can jeopardize the capacity and cycle life of the cell by consuming salt and solvent species, and compromises the safety of the system by generating gaseous products which increase the internal pressure of the cell. Minimizing the electrolyte reduction reactions and the capacity losses related to these processes is a major requirement for enhancing cycle life and improving the high-temperature performance of lithium-ion batteries. Electrolyte reduction is an expected feature of all cells using carbon-based insertion electrodes due to the instability of the electrolyte to the carbon electrode under cathodic conditions. The process of carbon passivation during the initial cell cycling is referred to as the formation period as discussed earlier. Ideally, electrolyte reduction is confined to the formation period and does not continue during the steady cycling of the cell.

Electrolyte reduction reactions on carbon surfaces are similar to those on lithium metal because the difference in potential between the metallic lithium and fully lithiated carbon is very small.[91] For this reason, a large amount of literature on electrolyte reduction processes on metallic lithium can be utilized to understand these processes on carbon insertion electrodes. A large number of experimental techniques including X-ray photoelectron spectroscopy (XPS), Auger electron spectroscopy, energy dispersive X-ray analysis (EDAX), Raman spectroscopy, on-line mass spectroscopy, in situ and ex situ Fourier transform infrared (FTIR) spectroscopy, atomic force microscopy (AFM), and electron spin resonance have been used to determine the reduction mechanisms and to identify the products formed on carbon electrode surfaces.[41,92-97]

Dey[92] studied the electrochemical decomposition of PC on graphite and proposed a decomposition mechanism

$$2Li^+ + 2e^- + (PC/EC) \rightarrow [propylene(g)/ethylene(g)] + Li_2CO_3(s) \quad [24]$$

The above reaction occurs during the first discharge when the potential of the electrode is near 0.8 V vs. Li/Li^+. Fong et al.[42] proposed a similar mechanism for the irreversible capacity loss during the first cycle on graphitic carbon electrodes with mixed EC/PC electrolytes.

Aurbach and coworkers[91,93,97] have performed extensive studies of solvent and salt reduction processes and their products on metallic lithium and carbon-based electrodes in a variety of electrolytes. They observed $ROCO_2Li$ species [probably $CH_3CH(OCO_2Li)CH_2OCO_2Li$] and propylene resulting from a one-electron reduction process of PC. Previously, Dey stated that PC reduction on graphite is a two-electron process with Li_2CO_3 and propylene as major products. Aurbach has argued that $ROCO_2Li$ species are highly sensitive to trace water and react rapidly with it to form Li_2CO_3, suggesting that previous studies were not conducted under sufficiently dry conditions.

In the presence of crown ethers,[91,95] carbon electrodes retain their graphitic structure and undergo reversible intercalation because the solvent is not cointercalated and reduced within the carbon, but rather on the surface. When the reduction of PC takes place on the surface, the charge transfer occurs mostly through existing films, and one would expect a one-electron reduction to be favorable because the driving force for PC reduction diminishes. In

previous studies,[92] graphite electrodes were destroyed and exfoliated in the absence of crown ethers, and did not reach intercalation stages when PC was the solvent. Thus, most of the PC reduction in that case could take place within the carbon structure after cointercalation of PC molecules into the graphite. In such a case, two-electron processes to form Li_2CO_3 may become favorable.

Matsumara et al.[94] observed that the irreversible capacity loss during the first cycle is not only due to PC decomposition to Li_2CO_3, but also because of additional side reactions. They concluded that during the first charge, it is possible that there are two paths for the decomposition of PC. In one, PC directly undergoes reduction to form propylene and Li_2CO_3. In the other, PC undergoes reduction to form a radical anion, and then forms lithium alkyl carbonates by radical termination. These are unstable and can be reduced to form unstable radical compounds that then react with propylene to form oligomer radicals, and finally oxidize to compounds which contain C-H bonds and COOH groups.

Shu et al.[95] studied the electrochemical intercalation of lithium into graphite in a 1 M $LiClO_4$ PC/EC (1:1) electrolyte. They suggested that two processes are involved, namely, a two-electron reduction of PC and EC to propylene and ethylene gases and one-electron reduction to form lithium alkyl carbonates. The two-electron reduction can be further divided into direct electrochemical and chemical reduction. The initial step for both electrochemical reduction and solid electrolyte interphase (SEI) film formation processes involves formation of lithium carbonate complexes followed by one-electron reduction to a radical anion. The radical anions undergo further one-electron reduction yielding gaseous products or radical termination to form an SEI film.

Chu et al.[96] used in situ electrochemical atomic force microscopy to study the surface films formed on highly ordered pyrolytic graphite (HOPG) electrodes during cathodic polarization in 1 M $LiClO_4$ EC/DMC (1:1) and 1 M $LiPF_6$ EC/DMC (1:1) electrolytes. They found the reduction reactions to be irreversible and suggested that these reactions occur on edge surfaces of HOPG at a higher potential (1.6 and 2.0 V vs. Li/Li^+) than on the basal surface (0.8 and 1.0 V). Peled[98] has also shown that more solvent reduction occurs on the basal surface and more salt reduction occurs on the edge surface. Chu showed that the surface film formed over the electrode is much thicker (a few hundred nanometers) than previously believed (10 nm at the basal surface and 50% thicker on the edge surface).[96]

A number of film-forming additives with beneficial properties have been discussed in the literature. The addition of large amounts of SO_2 promotes the reversible intercalation-deintercalation of lithium ions into graphite in selected nonaqueous electrolytes.[99] SO_2 offers the advantage of forming fully developed passive films on the graphite electrode at potentials much higher than that of electrolyte reduction itself. These passive layers are composed of Li_2S and Li-oxysulfur compounds as follows

$$SO_2 + 6Li^+ + 6e^- \rightarrow 2Li_2O + Li_2S \quad [25]$$

$$Li_2O + SO_2 \rightarrow (LiO)_2SO \quad [26]$$

or

$$Li_2O + 2SO_2 \rightarrow (LiO)OSOSO(LiO) \quad [27]$$

Carbonate-based mixed electrolytes containing DEC and DMC were found to undergo ester exchange reactions, which lead to the spontaneous formation of methyl ethyl carbonate.[100] This solvent has been disclosed in the patent literature as having desirable passivation properties for lithium-ion cells.[101] A recent study conducted on graphite electrodes in methyl propyl carbonate (MPC) solutions containing $LiPF_6$ or $LiAsF_6$ showed that the reduction of this solvent is initiated at potentials at or below 1.5 V vs. Li/Li^+. The authors observed Li_2CO_3 as a major surface species on the graphite electrode.

A new solvent mixture composed of chloroethylene carbonate (CEC), PC, and EC has been proposed for lithium-ion batteries.[102,103] CEC forms a stable passive film on the negative electrode which is insoluble in the electrolyte. This solvent allows the use of PC-based electrolytes with graphitic electrodes without increasing electrolyte decomposition. The recent patent literature contains references to other carbonate-based solvents, including other halogen-substituted carbonates and a variety of unsaturated carbonates, claimed to have desirable properties for lithium-ion batteries. Often these carbonates are added to the cell in small quantities and are involved and consumed in the initial reduction and film formation process at the carbon electrode. It is expected that work in this area will continue and that the understanding of the passive film composition and its relationship to battery performance will improve in the future.

A number of mechanisms have been proposed for the reduction of carbonate-based electrolytes (solvents and salts). These mechanisms (Eq. 28 to 46) are grouped based on solvents, salts, and contaminants.

Solvent reduction.—Propylene carbonate (PC).—The two-electron reduction mechanism of Dey[92] is

$$PC + 2e^- \rightarrow \text{propylene} + CO_3^{2-} \quad [28]$$

The one-electron mechanism for PC reduction given by Aurbach is

$$PC + e^- \rightarrow PC^- \text{ radical anion}$$

$$2PC^- \text{ radical anion} \rightarrow \text{propylene} + CH_3CH(CO_3^-)CH_2(CO_3^-)$$

$$CH_3CH(CO_3^-)CH_2(CO_3^-) + 2Li^+ \rightarrow CH_3CH(OCO_2Li)CH_2OCO_2Li(s) \quad [29]$$

(Li alkyl carbonate)

Ethylene carbonate (EC).—The two-electron reduction of EC is similar to that for PC

$$EC + 2e^- \rightarrow \text{ethylene} + CO_3^{2-} \quad [30]$$

and the one-electron mechanism is also analogous to the PC case

$$EC + e^- \rightarrow EC^- \text{ radical anion}$$

$$2EC^- \text{ radical anion} \rightarrow \text{ethylene} + CH_2(OCO_2)^-CH_2(OCO_2)^-$$

$$CH_2(OCO_2)^-CH_2(OCO_2)^- + 2Li^+ \rightarrow CH_2(OCO_2Li)CH_2OCO_2Li(s) \quad [31]$$

(Li alkyl carbonate)

The EC reduction product $CH_2(OCO_2Li)CH_2OCO_2Li(s)$ acts as an efficient passivating layer and is comparable to Li_2CO_3 in this respect.

Dimethyl carbonate (DMC).—This mechanism can be written as follows[91,104]

$$CH_3OCO_2CH_3 + e^- + Li^+ \rightarrow CH_3OCO_2Li + CH_3^\bullet \quad [32]$$

or

$$CH_3OCO_2CH_3 + e^- + Li^+ \rightarrow CH_3OLi + CH_3OCO^\bullet \quad [33]$$

Both CH_3OLi and CH_3OCO_2Li are formed by a nucleophilic attack on the DMC. The radicals formed ($CH_3^\bullet$ and $CH_3OCO^\bullet$) are converted to $CH_3CH_2OCH_3$ and $CH_3CH_2OCO_2CH_3$ as shown by Aurbach et al.[105]

Diethyl carbonate (DEC).—This mechanism can be written as follows[91,104]

$$CH_3CH_2OCO_2CH_2CH_3 + 2e^- + 2Li^+ \rightarrow CH_3CH_2OLi + CH_3CH_2OCO^\bullet \quad [34]$$

or

$$CH_3CH_2OCO_2CH_2CH_3 + 2e^- + 2Li^+ \rightarrow CH_3CH_2OCO_2Li + CH_3CH_2^\bullet \quad [35]$$

The radicals formed ($CH_3CH_2^{\bullet}$ and $CH_3CH_2OCO^{\bullet}$) by the decomposition of DEC are converted to $CH_3CH_2OCH_2CH_3$ and $CH_3CH_2OCO_2CH_2CH_3$ as shown by Aurbach et al.[104,106] Imhof and Novak[107] observed propylene and ethylene evolution on graphite electrodes in four different solvent mixtures (EC/DMC, PC/DMC, EC/PC, and EC/PC/DMC), but neither propylene nor ethylene were detected on nickel electrodes.

Salt reduction.—The salt used and its concentration should also affect the performance of carbon insertion electrodes, because salt reduction has been shown to participate in the buildup of surface films. In certain cases, salt reduction may contribute to stabilization of the surface and the formation of a desirable, passivating interface. In other cases, precipitation of salt reduction products may interfere with solvent reduction products. According to Jean et al.,[108] reduction of the lithium salt $LiCF_3SO_3$ occurs before solvent (PC/EC/DMC) reduction on the negative electrode.

The reduction reactions for the salts are as follows

$LiAsF_6$ [91,93]

$$LiAsF_6 + 2e^- + 2Li^+ \rightarrow 3LiF + AsF_3$$
$$AsF_3 + 2xe^- + 2xLi^+ \rightarrow Li_xAsF_{3-x} + xLiF \quad [36]$$

$LiClO_4$ [93]

$$LiClO_4 + 8e^- + 8Li^+ \rightarrow 4Li_2O + LiCl \quad [37]$$

or

$$LiClO_4 + 4e^- + 4Li^+ \rightarrow 2Li_2O + LiClO_2 \quad [38]$$

or

$$LiClO_4 + 2e^- + 2Li^+ \rightarrow Li_2O + LiClO_3 \quad [39]$$

$LiPF_6$ [91,104]

$$LiPF_6 \rightleftarrows LiF + PF_5$$
$$PF_5 + H_2O \rightarrow 2HF + PF_3O$$
$$PF_5 + 2xe^- + 2xLi^+ \rightarrow xLiF + Li_xPF_{5-x}$$
$$PF_3O + 2xe^- + 2xLi^+ \rightarrow xLiF + Li_xPF_{3-x}O$$

and

$$PF_6^- + 2e^- + 3Li^+ \rightarrow 3LiF + PF_3 \quad [40]$$

$LiBF_4$ (similar to $LiPF_6$) [91]

$$BF_4^- + xe^- + 2xLi^+ \rightarrow xLiF + Li_xBF_{4-x} \quad [41]$$

Contaminant reduction.—The electrolyte often contains contaminants such as oxygen and water. Oxygen can be reduced to form lithium oxide [93]

$$\frac{1}{2}O_2 + 2e^- + 2Li^+ \rightarrow Li_2O(s) \quad [42]$$

The performance of graphite electrodes is unaffected by small amounts of water (100 to 300 ppm) present in the solvents. For higher concentrations of water, LiOH is formed on reduction of water on graphite in the presence of Li^+, which precipitates on the surface of the carbon and acts as a blocking agent with a high interfacial resistance. Thus, LiOH can prevent further intercalation of Li^+ into graphite

$$H_2O + e^- \rightarrow OH^- + \frac{1}{2}H_2\uparrow$$
$$Li^+ + OH^- \rightarrow LiOH(s) \quad [43]$$
$$LiOH(s) + e^- + Li^+ \rightarrow Li_2O(s) + \frac{1}{2}H_2$$

In the presence of CO_2, Li_2CO_3 is formed as a passive layer on the negative electrode

$$2CO_2 + 2e^- + 2Li^- \rightarrow Li_2CO_3 + CO \quad [44]$$

or

$$CO_2 + e^- + Li^+ \rightarrow CO_2^-\cdot Li^+$$
$$CO_2Li + CO_2 \rightarrow OCOCO_2Li$$
$$OCOCO_2Li + e^- + Li^+ \rightarrow CO + Li_2CO_3 \quad [45]$$

Secondary reaction.—Lithium carbonate can also be formed by a secondary reaction[93]

$$2ROCO_2Li + H_2O \rightarrow 2ROH + CO_2 + Li_2CO_3 \quad [46]$$

where R = ethyl or propyl group. $LiAsF_6$ and $LiPF_6$ reduction (Eq. 36 and 40) occur at potentials less than 1.5 V (vs. Li/Li^+).[99]

Self-discharge Processes

Self-discharge refers to the drop in cell voltage under open-circuit conditions that occurs spontaneously while batteries are left standing. Lithium-ion batteries undergo self-discharge which, although less significant than those of the competing Ni-Cd and Ni-MH batteries, is still relatively rapid and temperature dependent. Self-discharge phenomena inevitably occur in oxidized $LiMn_2O_4$, $LiCoO_2$, and $LiNiO_2$ electrodes. The extent of this self-discharge depends on factors such as cathode and cell preparation, nature and purity of the electrolyte, temperature, and time of storage.

Self-discharge losses in lithium-ion cells have been classified according to whether they are reversible or irreversible.[38] Reversible capacity losses were defined as those that can be recovered by charging the cell again while irreversible capacity losses were not recoverable. While this is a useful practical distinction to make, the extent to which capacity loss is irreversible depends on the charge and discharge rates used on the subsequent cycling. Hence, capacity losses due to self-discharge should preferably be accompanied by statements of the rates at which the data were obtained. For purposes of discussing self-discharge mechanisms, we attempt to separate processes that might lead to true irreversible capacity losses (capacity that cannot be regained at any charge rate) from processes that should be readily reversible and lead to no permanent capacity loss.

Johnson and White[10] have reported the self-discharge behavior of Sony and Matsushita cells. They monitored the open-circuit potential of these cells for 30 days and observed that all the cells maintained capacities greater than 97% of their initial capacity. Thus, they concluded that the effect of self-discharge on capacity fade during cell cycling is insignificant. The self-discharge rate is very high (10%/month at 55°C) at high temperature compared to 2-3%/month at room temperature. The capacity loss due to self-discharge is mostly recoverable as reported in the literature.

The self-discharge mechanism[38,109-111] for $LiMn_2O_4$/organic electrolyte cells has been stated to involve irreversible electrolyte oxidation at the positive electrode and the reversible insertion of lithium into the $Li_yMn_2O_4$ spinel structure. The insertion process is reversible and the extent of delithiation of the electrode can be returned by recharging the cell. In general, charged lithium-ion cells can self-discharge by coupling the electrolyte-decomposition reaction to the primary lithium-intercalation reaction. The superficial oxidation[90] of the electrolyte at the positive electrode surface can be written as

$$El \rightarrow e^- + El^+ \quad [47]$$

where El can be any solvent (EC, PC, etc.) used in lithium-ion batteries. The released electrons are used by the metal oxides (positive electrodes) to intercalate lithium according to the reaction

$$yLi^+ + ye^- + MO_z \rightarrow Li_yMO_z \quad [48]$$

which is the bulk intercalation of lithium into the positive electrode structure leading to a decrease in the state of charge of the electrode. For $Li_xMn_2O_4$

$$Li_yMn_2O_4 + xLi^+ + xe^- \rightarrow Li_{y+x}Mn_2O_4 \quad [49]$$

The above reactions (Eq. 47 and 49) can occur simultaneously at the composite positive electrode without any external electron source. The overall reaction is

$$Li_yMn_2O_4 + xLi^+ + xEl \rightarrow Li_{y+x}Mn_2O_4 + xEl^+ \quad [50]$$

The rate of self-discharge is limited primarily by the rate of solvent oxidation, emphasizing the importance of solvent stability in long shelf-life batteries. Guyomard et al.[38] have demonstrated that solvent oxidation occurs mainly on the carbon black surface, and recommended low surface area carbon black for controlling self-discharge rates. However, reducing the surface area of the active material has also been stated as important in this regard in the case of $LiMn_2O_4$, and the role of the current collector surface in carrying out solvent oxidation cannot be dismissed.

The self-discharge of the positive electrode as written above would cause a permanent loss of capacity if the anode retained its charged state. This is a result of the perturbation of the capacity balance in the cell implicit in these mechanisms. Fortunately, self-discharge data recorded with a lithium reference electrode indicated that each electrode in the lithium-ion cell may self-discharge at a similar rate as in the manganese oxide-carbon case.[38] The salt concentration in the cell can also be changed irreversibly by these processes. Either of these phenomena will lead to capacity or rate capability losses over the life of the cell. After long or repeated self-discharges, the lithium-ion cell will have unbalanced capacities in the two electrodes with an increased risk of lithium plating on carbon during charging.

Further studies of self-discharge phenomena in lithium-ion cells were undertaken by Pistoia et al.[110,111] The self-discharge rates of the three main metal oxide cathodes were compared to one another in various electrolyte systems. Electrolyte oxidation was again involved in the self-discharge mechanism, although this process alone could not explain all of the experimental findings. Self-discharge rates varied widely in different electrolytes as would be expected from the electrolyte oxidation mechanism. In addition, the consequences of pore pluggage by oxidation products after self-discharge periods were seen in some cases, including higher internal resistance and losses of rate capability.

Two additional mechanisms for self-discharge were proposed, one being the spontaneous lithium reinsertion into the positive electrode driven by the negative electrode and the second being electrode dissolution.[111] The former process was ascribed to the partial instability of the oxidized positive electrode. Interestingly, this process halted when the lithium-metal negative electrode was replaced by a platinum electrode, leading the authors to conclude that lithium ions from the negative electrode were involved in the self-discharge process. Because no net flow of current can exist during self-discharge, a flux of lithium ions from the negative to positive electrode must be compensated by an equal and opposite flux of another ionic species between the electrodes. This could be the result of either solvent oxidation at the positive electrode (leading to generation of cations) or solvent reduction at the lithium-metal electrode. The second mechanism, which is discussed in more detail in a later section, can be controlled by the proper choice of electrolyte.

During self-discharge, delithiation of lithiated coke (and graphite) can be explained by the following redox process, which is obtained by coupling the electrolyte decomposition reaction and lithium insertion reaction at the negative electrode[38]

$$El + ye^- \rightarrow \text{passivating layer } Li_xC_6 - ye^- - yLi^+ \rightarrow Li_{x-y}C_6 \quad [51]$$

In this case, the electrolyte reduction reaction is thermodynamically possible due to the very reducing potential (a few hundreds of millivolts vs. Li/Li^+) but is kinetically slow due to the already existing passivating layer on the negative electrode surface. As stated above, the rates of the self-discharge processes on the two electrodes in this study were similar, leading to little permanent capacity loss.

The majority of the self-discharge observed in commercial lithium-ion cells is reversible with only a very small fraction irreversible. The mechanisms proposed in the literature (coupled electrolyte decomposition, discussed above) lead to irreversible losses in many cases because of the consumption of cyclable lithium (to form products such as lithium carbonate) or the physical blockage of active electrode surface area. Self-discharge mechanisms which do not lead to permanent capacity loss are needed. One possible process would be the transport of oxidized solvent species from the positive to negative electrode where reduction would occur, in other words, a redox shuttle process. These species could be reversibly oxidized and reduced similar to internal shuttle mechanisms discussed earlier, or could be destroyed upon reduction adding to the carbon electrode's natural passivation layer. As long as the same number of electrons were involved in both the oxidation and reduction processes, the cell's capacity balance would survive these processes and the self-discharge would be recoverable.

Another reversible contribution to self-discharge in lithium-ion cells can be attributed to the leakage currents through the separator of the cell. This leakage current may be increased due to any number of imperfections in the manufacturing process, such as pinholes in the separator. Because of the need to conserve current flow, leakage currents due to finite separator electronic conductivities are balanced by the electrochemical discharge of the cell. This process would likely occur at very low rates, limited only by the electronic resistance of the separator. Because this process is expected to be only weakly dependent on temperature, the fact that experimental self-discharge data on lithium-ion cells are strongly temperature dependent suggests this mechanism is not a primary one.

Interfacial Film Formation

A passive film is formed at the negative electrode/electrolyte interface because of irreversible side reactions that occur between lithium ions and/or the solvent and electrode surface (see Eq. 28 to 46). Certain aspects of these processes were discussed in previous sections. These side reactions will ideally form a stable, protective film on the negative electrode allowing the electrode to continue to operate without further reaction. The initial loss of lithium ions in forming this film causes the capacity balance between the two electrodes to change. This may result in a diminished utilization and hence a decreased specific energy for the entire battery. The irreversible capacity loss with carbon electrodes can vary between 10 and 100% of the reversible capacity for different types of carbon. The capacity lost depends on the type of carbon used, the components of the electrolytic solution, and additives to the electrode or solution. Passive film formation is different than lithium deposition which occurs during negative electrode overcharge. The passive film can form on either electrode and consists of products (Li_2CO_3, etc.) formed by electrolyte decomposition.

Peled[50,51,112-114] has explained many of the fundamental processes taking place at the lithium and lithiated carbon electrode/electrolyte interfaces and has put forth models to explain these interfacial phenomena. The solid electrolyte interphase (SEI) passivation layer on the carbon surface plays a major role in determining electrode and battery behavior and properties including cycle life, shelf life, safety, and irreversible capacity loss. The major role of the SEI is to separate the negative electrode from the electrolyte, to eliminate (or to reduce) the transfer of electrons from the electrodes to the electrolyte, and also the transfer of solvent molecules and salt anions from the electrolyte to the electrodes. The actual morphology of the SEI is very complex and changes with time and with electrolyte composition. It is best described as a thin heterogeneous film

of a mosaic of numerous individual particles of different chemical compositions in partial contact with each other at grain boundaries.[50] The SEI passivating layer over metallic lithium is a more porous or structurally open layer of corrosion products which, to some extent, blocks the surface of the anode and do not take part in the deposition-dissolution process.

When a carbonaceous electrode is cathodically polarized to potentials lower than 2 V vs. Li/Li^+, many side reactions take place simultaneously as shown in Fig. 5. Peled studied the lithium metal/polymer electrolyte interface in detail. The polymer electrolytes used were LiI-PEO-Al_2O_3 based composites. He found that a single parallel RC element representing the apparent resistance (R_{SEI}), apparent capacitance (C_{SEI}), and apparent thickness (L_{SEI}) of the SEI layer could be used to fit the impedance response of the interface and predicted a parabolic growth rate for SEI films.[50] The proposed model cannot be generalized to conditions outside the ones on which they have been derived and therefore cannot be used to develop detailed design specifications. A more comprehensive and general model based on first principles needs to be developed which will be valid for lithium-ion electrodes under varying conditions.

The deposition-dissolution process of a solid electrolyte interface film involves three consecutive steps: (*i*) electron transfer at the metal/solid electrolyte interface; (*ii*) migration of cations from one interface to the other; (*iii*) ion transfer at the solid electrolyte/solution interface.

$$M - ne^- \rightarrow M^{n+}_{M/SE} \quad [52]$$

$$M^{n+}_{M/SE} \rightarrow M^{n+}_{SE/sol} \quad [53]$$

$$m(solv) + M^{n+}_{SE/sol} \rightarrow M^{n+}\cdot m(solv) \quad [54]$$

The rate-determining step for the deposition-dissolution process is often the migration of lithium cations through the passivating layer covering the lithium surface.[115,116]

The passive film formation over the electrode can be explained by a simple heterogeneous reaction between the electrolyte solvent (El) and Li_xC_6 [117]

$$Li_xC_6 + \delta El = \delta LiEl + Li_{x-\delta}C_6 \quad [55]$$

The SEI model assumes that the passive layer formed over the surface prevents further reaction but still allows lithium ions to pass through. The above reaction can be separated into two steps

$$Li_xC_6 = Li_{x-\delta}C_6 + \delta Li^+ + \delta e^- \quad [56]$$

$$\delta Li^+ + \delta e^- + El_{(liquid)} \rightarrow \delta LiEl_{(solid)} \quad [57]$$

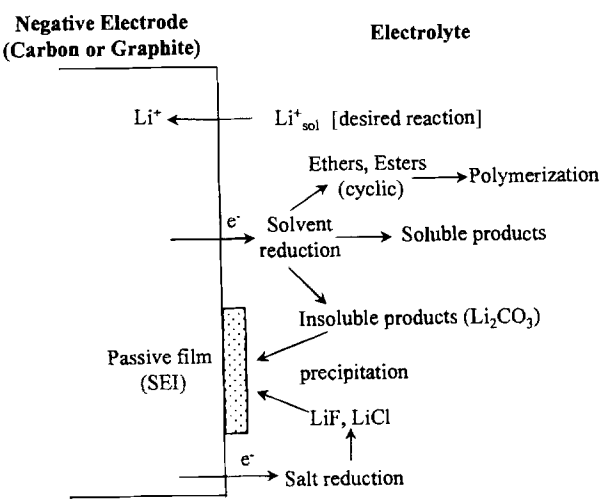

Fig. 5. The complexity of the intercalation process in the negative electrode.

The above two reactions show that the process will proceed only if electrons are transferred through the film from the carbon to the SEI/electrolyte interface, or if solvent molecules are transferred from the electrolyte to the SEI/carbon interface. Solvent molecules could penetrate the film either through imperfections, such as cracks, or if they are sufficiently mobile through the bulk of the SEI film.

Garreau et al.[118] have proposed a polymer electrolyte interphase (PEI) model to describe the behavior of the lithium metal electrode covered by a porous nonconducting polymeric film. The charge-transfer reaction is limited by the surface coverage of the lithium electrode by the PEI and with the diffusion of electrolyte through the porous structure of the interface. The composition of the electrolyte is a determining factor in the nature of the passivating film formed. The carbonate-based solvents react with the carbon, lithium, or lithiated carbon to form alkene gases and Li_2CO_3 as the primary film-forming material, as discussed earlier in the solvent decomposition section.

Current Collectors

Copper and aluminum are the most commonly used current collectors for negative and positive electrodes, respectively. In addition to these metals, nickel and stainless steel have also been tested for current collectors in lithium-ion cells. The main issues related to current collectors are passive film formation, adhesion, localized corrosion such as pitting, and general corrosion. These phenomena increase the internal impedance of the cell during cycling and can lead to capacity and rate capability losses. There are still relatively few studies of corrosion processes in lithium-ion cells; however, as the challenges in this area receive more attention, more work and advances in understanding can be expected.

Both current collectors in lithium-ion cells are susceptible to degradation, with Al to pitting corrosion and Cu to environmentally assisted cracking.[119] The pitting of aluminum in PC/DEC and EC/DMC electrolytes was studied using impedance spectroscopy, XPS, and Auger techniques by Braithwaite and coworkers.[119,120] Al became more passive on cycling, and Li and P were the predominant surface species observed on the Al surface. These authors demonstrated that chromate conversion coatings provide good protection to Al in lithium-ion cells. Environmental cracking of Cu can occur at or near the lithium potential if specific metallurgical conditions exist such as work hardening. The passive film on the copper current collector in these environments was relatively thin (<150 Å) and did not appear to thicken during cycling.

Recently Pistoia et al.[121] reported that $LiPF_6$-EC/DMC electrolytes corrode Al nets at 3.1 to 3.2 V and Al foils at 4.2 V vs. Li/Li^+ depending on their HF content. In $LiBF_4$-EC/PC and $LiClO_4$-EC/DMC, Al foils do not corrode below 4.9 V, and on graphitized Al several electrolytes can withstand potentials above 4.5 V. Chen et al.[122] examined Al current collectors using scanning electron microscopy (SEM) after charging at various potentials in lithium/poly(ethylene oxide)-$LiN(CF_2SO_3)_2/V_6O_{13}$ or TiS_2 cells. They observed pitting corrosion on Al current collectors which affects the long-term reliability of lithium-polymer batteries. An alternate corrosion-resistant W-Al alloy was proposed which forms a more protective corrosion product film over the current collector surface.

Both of the current collectors in commercial lithium-ion cells are pretreated (acid-base etching, corrosion-resistant coatings, conductive coatings, etc.) to improve their adhesion properties and to reduce corrosion rates. These pretreatments help significantly for both Al and Cu current collectors. In the case of Al, operation without any prior surface treatments leads to substantial increases in interfacial resistance over the life of the battery. Loss of current collector adhesion can dramatically impact cell capacity because portions of the electrode may become totally disconnected from the conducting matrix. With Cu, disconnected regions can even promote lateral variations in electrode potential which may force lithium deposition to occur.

Current collector corrosion can lead to an increase in the battery's internal resistance over many cycles due to the formation of an insulating film of corrosion products on the surface of the current collector. The increase in internal resistance depends critically on the treatments used on the current collector interface prior to cell assembly and causes the battery to lose some power capability later in its life. A loss in rate capability (or increase in internal resistance) can lead indirectly to capacity loss when the capacity is assessed at a given rate.

The dissolution of the copper current collector is a possible overdischarge reaction at the negative electrode (Fig. 3)

$$Cu \rightarrow Cu^{+} + e^{-} \quad [58]$$

Univalent copper is more likely than divalent in a nonaqueous environment.[123] The thermodynamic equilibrium potential for this reaction in an aqueous solution under standard conditions is 0.521 V vs. SHE or 3.566 V vs. Li/Li^{+}. The potential of carbon-based negative electrodes near the end of discharge or under overdischarge conditions may reach in excess of 1.5 V vs. Li/Li^{+}. Apparently, this reaction occurs much more readily than expected because of the nonaqueous environment in the cell, where standard thermodynamic data taken in aqueous media no longer hold.

The copper ions that are formed on overdischarge can redeposit later as copper metal at the negative electrode, forming dendrites which may penetrate the separator and cause cells to fail catastrophically. These processes generally prevent lithium-ion cells from being discharged below approximately 2.5 V. This is a serious problem in bipolar stacks of cells as it is difficult to control each individual cell voltage. Thus, a cell may be overdischarged because it has a lower capacity, and this could destroy the whole stack. For other consumer electronics applications, it would be advantageous for lithium-ion cells to have better overdischarge tolerance.

Positive Electrode Dissolution

Positive electrode dissolution phenomena are both electrode and electrolyte specific, and limited data on these processes are available for most materials. The factors determining positive electrode dissolution are structural defects in the positive active material, high charging potentials, and the carbon content in the composite positive electrode. Oxygen defects in the $LiMn_2O_4$ and $LiNiO_2$ structures may weaken the bonding force between the transition metal and oxygen, resulting in Mn and Ni metal dissolution. The transition metal ions which have weak bonding forces with oxygen could be driven into the electrolyte, especially when polarized to high potentials.[66] Electrolyte oxidation on the carbon black surface may generate catalytic species which can increase the rates of metal-ion dissolution.

Of the three main high-voltage metal oxide positive electrode materials, cation dissolution has been most studied to date on the lithium manganese oxide spinel. Dissolution of the $LiMn_2O_4$ active material occurs through a disproportionation mechanism leading eventually to manganese deposition on the negative electrode. This causes a loss of positive active material and blocking of pores in the negative electrode. The Mn^{2+} dissolution reaction is believed to occur when the $LiMn_2O_4$ electrode is fully discharged, and can be a major problem in the shelf life of discharged cells. These processes have been studied by a number of authors including Thackeray and coworkers and the Bellcore research group.[124-128]

The capacity fading upon cycling was first ascribed to the dissolution of Mn by Thackeray.[128] Tarascon and coworkers detected the presence of Mn on the surface of the negative electrode by Rutherford backscattering spectroscopy (RBS).[127] Wen et al.[129] reported that the capacity fade on cycling in the higher voltage region was attributed to the fact that the active electrode material was gradually converted to a lower voltage defect spinel phase via the dissolution of Mn into the electrolyte. Recently Xia et al.[130] reported that capacity loss caused by the simple dissolution of Mn^{3+} accounted for only 23 and 34% of the overall capacity loss observed at room temperature and 50°C, respectively. They suggested that the rest of the capacity fade originated from structural changes and decomposition of the electrolyte solution.

According to Bellcore[124,127,131] and Dahn,[52,132] 25% of the Mn^{2+} dissociated ends up depositing on the negative electrode surface. This occurs via the following mechanism[52,124,127,131-135]

$$4H^{+} + 2LiMn^{3+}Mn^{4+}O_4 \rightarrow 3\lambda - MnO_2 + Mn^{2+} + 2Li^{+} + 2H_2O \quad [59]$$

which is the acid-induced decomposition of the spinel.[134] This disproportionation process is due to the instability of the Mn^{3+} oxidation state, which reacts spontaneously to form Mn^{2+} and Mn^{4+}. Mn^{2+} then goes into solution and redeposits as Mn(s) at the negative electrode

$$Mn^{2+} + 2e^{-} \rightarrow Mn(s) \quad [60]$$

It could also be the case that colloidal $LiMn_2O_4$ particles move toward the negative electrode by electrophoresis and deposit manganese at the negative electrode. However, if electrophoresis were taking place, the amount of manganese determined at the negative electrode should depend strongly on the particle size of the electrodes, which was not the case.

The above reaction (Eq. 59) is greatly accelerated with increasing temperature. The protons arise from HF, which originates with the hydrolysis of $LiPF_6$ salt and thus depends critically on $LiPF_6$ purity[97]

$$H_2O + LiPF_6 \rightarrow POF_3 + 2HF + LiF \quad [61]$$

The water produced by the Eq. 59 can also generate more protons, making the manganese dissolution process autocatalytic in nature. Free protons could also be consumed at the negative electrode via

$$2H^{+} + 2e^{-} \rightarrow H_2(g) \quad [62]$$

The Mn^{2+} dissolution reaction can be reduced or slowed by using high purity $LiPF_6$ and low surface area $LiMn_2O_4$ ($<1\ m^2/g$).[136,137] Limiting the surface area also reduces the catalysis of side reactions such as solvent oxidation. There is experimental evidence that the hexafluorophosphate anion is more directly involved in the manganese dissolution process, perhaps through an anion-assisted mechanism.[138]

Jang et al.[139] stated that manganese dissolution is the primary reason for capacity losses in $LiMn_2O_4$ electrodes. In this study, manganese dissolution brought about an increase in contact resistance at the manganese-depleted-spinel/carbon interface and also increased the electrode reaction resistances for lithium insertion-deinsertion. They reported experimental data for the dependence of manganese dissolution on applied potential. The dissolution rate was not appreciable when the applied potential was below ca. 4.0 V vs. Li/Li^{+}, but it became notably high above 4.0 V. According to these authors, the disproportionation mechanism (Eq. 59) seems unlikely to be a cause for the dissolution because dissolution was seen predominantly at the end of the charging process, in which potential range the Mn^{3+} content in the spinel is minimal.

In another study, Jang and Oh[140] reported that spinel dissolution is induced by acids that are generated as a result of electrochemical oxidation of solvent molecules on composite cathodes. The spinel dissolution was much higher in the ether-containing electrolytes such as DME and THF as compared to the carbonates. In the initial stages only Li and Mn ions are extracted, while in the later stages oxygen loss becomes dominant. They found that solvent-derived acid generation was not significant in electrolytes containing fluorinated salts ($LiPF_6$, $LiBF_4$, and $LiAsF_6$), yet the spinel dissolution in these electrolytes

was appreciable because the acids are generated by the reaction between the F^- containing anions and impurity water (such as Eq. 61 above).

Although the results of Jang et al. appear contradictory to the earlier work, it is likely that a similar mechanism is operating in all cases. Jang et al. have emphasized the important link between the generation of protons in the cell and manganese dissolution. By using ether-based solvents, a much larger quantity of protons is generated thus leading to higher rates of manganese dissolution than would have been seen in earlier studies with oxidation-resistant carbonate solvents. The link between manganese dissolution and electrode potential is due to this potential-dependent solvent oxidation process, not the state-of-charge of the positive electrode as suggested by Jang et al.

Robertson et al.[141] also proposed an alternate mechanism for spinel dissolution. They proposed that a modified proton-catalyzed redox mechanism is responsible for Mn extraction from the cathode and the concurrent formation of Li_yMnO_x species which were electrochemically inactive at 4 V

$$12LiMn_2O_4 \rightarrow Li_2MnO_3 + 5Li_2Mn_4O_9 + 3Mn^{2+}_{solv} \quad [63]$$

$$12Mn^{3+} \rightarrow 9Mn^{4+} + 3Mn^{2+}_{solv} + 6e^- \quad \text{oxidation} \quad [64]$$

$$3Mn^{2+}_{solv} + 6e^- \rightarrow 3Mn\downarrow \quad \text{reduction} \quad [65]$$

Li_2MnO_3 is electrochemically inert, and $Li_2Mn_4O_9$ has virtually no capacity in the 4 V region. From Eq. 63 to 65, 12 M of $LiMn_2O_4$ become inactive for every 3 M of Mn^{2+} that dissolve into the electrolyte. Moreover, $Li_2Mn_4O_9$ cycles in the 2 to 3 V domain. They suggested that low levels of Cr^{3-} in the spinel framework can substantially reduce cathodic manganese dissolution into the electrolyte.

Based on the evidence for the dissolution of manganese and the change in crystal structure of the spinel during cycling, Xia et al.[130] proposed that manganese dissolves via two routes: (*i*) $LiMn_2O_4$ is transformed to $LiMn_{2-x}O_{4-x}$, via loss of MnO, and, (*ii*) $LiMn_2O_4$ is transformed to $Li_{1+x}Mn_{2-x}O_4$, via loss of Mn_3O_4. For the first case, a portion of Mn^{3+} transforms to Mn^{4+} together with dissolution of MnO into solution, i.e.

$$Mn^{3+}(LiMn_2O_4) \rightarrow Mn^{4+}(Li_2Mn_3O_7) + Mn^{2+}(MnO) \quad [66]$$

Amatucci et al.[142] reported a strong and direct relationship between capacity loss and percentage of cobalt detected on the negative electrode for $LiCoO_2$-based lithium-ion cells charged above 4.2 V. The capacity loss (or Co dissolution) depended on the thermal treatment during synthesis of the active material. Cobalt ions present in the electrolyte after dissolution are reduced at the negative electrode. The rate of dissolution increases with cutoff voltage, with a steep increase when the cutoff voltage is 4.5 V. A quantitative relationship between the percentage of cobalt dissociated and capacity loss for $LiCoO_2$ cells with a cutoff (charging) voltage of greater than 4.2 V was given by these authors.

In certain lithium-vanadium oxide ($Li_yV_2O_5$) cells based on an $LiAsF_6$-EC/PC/2Me-THF (15:70:15) electrolyte, vanadium was found to dissolve partially and then plate on the lithium electrode leading to an increase in cycle life.[143] The vanadium incorporated into the lithium surface film was shown to be beneficial to the passive film properties in this electrolyte. This work demonstrates the electrode material and cell-specific nature of the dissolution process and its impact on battery performance.

Phase Changes in Insertion Electrodes

The understanding of the relationship between phase changes in insertion electrodes and capacity loss is weak even though this is widely quoted as a mechanism of capacity loss. The basic mechanism stated is that phase changes or large changes in lattice parameters leads to fracture of particles and loss of contact from the electrode matrix. In general, one might believe that good electrodes showing high reversibility and cycle life probably are not accompanied by significant phase changes or lattice expansion or contraction during operation. The three main metal oxide insertion compounds most studied currently for lithium-ion batteries are in this category. However, the constant search for higher capacity materials makes phase changes and structural changes difficult to avoid, and the effects of these processes on battery performance is only beginning to be quantified and studied in a fundamental manner.

The phase changes occurring in lithium-ion cells can be classified into two types: those that occur during normal insertion-deinsertion of lithium, and others that occur when the positive electrode is overcharged or overdischarged (for example, the Jahn-Teller distortion[144] in the case of overdischarge of $Li_yMn_2O_4$ above $y = 1$).[145] Xia et al.[145] and Ohzuku et al.[144] have studied the phase changes occurring in spinel $LiMn_2O_4$ electrodes. Xia et al. concluded that the transformation of unstable two-phase to a more stable one-phase structure occurs via loss of MnO ($Mn^{3+} \rightarrow Mn^{4+} + MnO$), which dominates the capacity fading during the room temperature cycling of cells.

Amatucci et al.[124] described the insertion of lithium into $LiMn_2O_4$ as single phase and biphase. The biphase insertion scheme as proposed by them is

$$Li_yMn_2O_4 \xrightarrow{-Li^-} \lambda - Mn_2O_4 \xrightarrow{100\text{-}250^\circ C} \beta\text{-}MnO_2 \xrightarrow{+Li^+} LiMnO_2 \quad [67]$$

$$\lambda - Mn_2O_4 \rightarrow \epsilon - Mn_2O_4 \rightarrow \beta - MnO_2 \quad [68]$$

Delithiation of $Li_yMn_2O_4$ leads to formation of λ-Mn_2O_4 that decomposes to β-MnO_2 at temperatures ranging from 100 to 250°C, and in some cases ϵ-Mn_2O_4 may be detected as an intermediate in the process of decomposition. Rutile β-MnO_2 is electrochemically inactive at 4 V and leads to the formation of orthorhombic $LiMnO_2$ on lithium insertion. These phase changes during cycling may lead to capacity losses in practice. Recently, Cairns et al.[146] have used in situ X-ray adsorption techniques to determine that upon delithiation of $LiMn_2O_4$, the lattice contracts to a structure similar to λ-MnO_2, whereas lithiating $LiMn_2O_4$ transforms the cubic spinel into the tetragonal phase $Li_2Mn_2O_4$.

Another major reason for capacity fade in $LiMn_2O_4$ spinel-based cells is overdischarge leading to a lower than 3.5 average oxidation state for manganese.[127] This may cause a Jahn-Teller distortion of the $LiMn_2O_4$ structure that occurs when the oxidation state drops below 3.5.[127,146-148] During the Jahn-Teller distortion, the z axis stretches by 15% and the x and y axes contract by 6%. The large anisotropic expansion (16%) of the unit cell is too severe for the tetragonal $Li_2Mn_2O_4$ phase on the surface and cubic $LiMn_2O_4$ in the bulk to remain as one intergrown structure within a single crystallite. Particle fragmentation may result (giving higher surface area), causing the Mn^{3+} dissolution reaction to become more troublesome and leading to loss of contact between particles. This structural damage to the spinel electrode may lead to slow capacity loss on cycling.

The Jahn-Teller distortion process is greatly reduced by using an excess of lithium in the $LiMn_2O_4$ starting material ($x = 1.05$ or higher). Lithium substitution into manganese sites leads to an increase in the average oxidation state for the manganese. This has also been accomplished by doping $LiMn_2O_4$ with other atoms such as cation substitution with Fe or Co,[149-151] or anion substitution with F.[152,153] Lithium manganese oxide spinel electrodes stabilized in some manner to prevent overdischarge can exhibit constant capacity during cycling for several thousand cycles at room temperature.

Ohzuku et al.[144] concluded that the reduction of $Li_yMn_2O_4$ proceeds in three steps, which consist of a cubic/cubic two-phase reaction, a cubic one-phase reaction, and a cubic/tetragonal two-phase reaction as shown in Table II. A large voltage drop of 1 V is observed for $y > 1$, which is due to a Jahn-Teller distortion of MnO_6-octahedron from O_h symmetry to D_{4h} symmetry. According to these authors, the apparent stabilization energy of MnO_6-

Table II. Phase changes in positive electrodes during discharge.

Material	Region	U (V vs. Li/Li^+)	Phase	y in $Li_yMn_2O_4$	Ref.
$Li_yMn_2O_4$	I	2.96	One cubic and tetragonal	$1.0 < y < 2.0$	144
	II	3.94	One cubic	$0.6 < y < 1.0$	
	III	4.11	Two cubic	$0.27 < y < 0.6$	
Li_yCoO_2	I	4.0	Single hexagonal	$0.9 < y < 1.0$	142
	II	4.0	Two hexagonal	$0.78 < y < 0.9$	
	III	4.09	Single hexagonal	$0.51 < y < 0.78$	
	IV	4.2	Monoclinic	$0.46 < y < 0.51$	
	V	4.49	Hexagonal	$0.22 < y < 0.46$	
	VI	4.5	Hexagonal + monoclinic	$0.18 < y < 0.22$	
	VII	4.6	Monoclinic	$0.15 < y < 0.18$	
	VIII	5.0	Hexagonal	$0 < y < 0.15$	
Li_yNiO_2	I	3.65	Rhombohedral	$0.85 < y < 1$	161
	II	3.88	Monoclinic	$0.5 < y < 0.75$	
	III	4.15	Rhombohedral	$0.32 < y < 0.43$	
	IV	4.21	Two rhombohedral	$0 < y < 0.32$	

octahedron ($O_h \rightarrow D_{4h}$) results in a loss of 1 V. The abrupt change in unit-cell volume (6.5%) which accompanies the cubic-to-tetragonal phase transition in the spinel has a deleterious effect on the cyclability.[154] Ideally, tetragonal $LiMn_2O_4$ should be present at the end of each discharge. The cubic $LiMn_2O_4$ accumulated at the end of discharge is the primary cause of the significant loss in capacity.

A number of other lithium manganese oxide structures have been synthesized and tested for insertion-deinsertion capacity and reversibility over the past several years.[125,127,155-160] In general, these compounds revert to the spinel structure over the course of cycling due to the strong driving force to achieve the thermodynamically most stable phase. These phase changes are often also accompanied by capacity losses, although the mechanisms for these losses probably vary from case to case.

Phase changes are also observed in the case of $LiCoO_2$ and $LiNiO_2$ electrodes.[142,154,161] The different phases and the corresponding y values for both electrode materials are given in Table II. In the case of $LiCoO_2$, various hexagonal and monoclinic phases are observed, whereas in the case of $LiNiO_2$, monoclinic and rhombohedral phases are formed. Although phase changes occur in these electrodes, they have not been associated with capacity losses. The Li_yNiO_2 electrode is usually cycled between $y = 0.3$ and 0.9, whereas Li_yCoO_2 is cycled between $y = 0.5$ and 1.0, to avoid significant phase changes during cycling. Gummow and Thackeray synthesized LT-$LiCo_{0.9}Ni_{0.1}O_2$ with a structure that is intermediate between an ideal lithiated spinel and a layered structure.[162] They reported improvements in electrochemical performance and attributed it to the formation of a defect spinel phase $Li_{0.8}[Co_{1.6}Ni_{0.2}]O_4$ in which the lithium ions adopt the tetrahedral A sites and the cobalt and nickel ions the B sites of an $A[B_2]O_4$ spinel.

In carbon insertion electrodes, during the charging cycle a reversible expansion of interlayer spacing occurs along the c axis.[163] Lithium intercalation in graphite shows a structural transformation[43] from the ABA to the AAA structure. These structural changes in graphite electrodes during intercalation/deintercalation of lithium have not usually been associated with capacity losses.

Incorporation of Capacity Fade Mechanisms into Battery Modeling

Modeling capacity fading and failure mechanisms requires that side reactions be incorporated into a general lithium-ion battery model. The basic procedure for accomplishing this is discussed here; followed later by some elaboration within the context of particular capacity fade mechanisms. Either heterogeneous or homogeneous reactions can be included, although only heterogeneous electrochemical side reactions are treated here. Past battery modeling work on other systems has included many of the phenomena discussed here, such as the incorporation of the oxygen evolution side reaction into nickel-cadmium and lead-acid battery models.[164-168] The basic approach to incorporating side reactions is to write a rate expression for the side reaction in question and material balances for each species involved in the reaction. Various approximations might be used to reduce the number of equations beyond this point. A thorough discussion of the macroscopic approach to full-cell sandwich battery modeling can be found in the literature.[169-171]

A general electrochemical side reaction can be expressed as

$$\sum_i s_i M_i^z \rightarrow ne^- \qquad [69]$$

where s_i is the stoichiometric coefficient of species i and n is the number of electrons transferred in the reaction. Because the rate of side reactions will often be kinetically limited, we first discuss the formulation of kinetic rate expressions for electrochemical reactions. A Butler-Volmer-type rate expression is written for each reaction as

$$i_k = i_{o,k}\left[\exp\left(\frac{\alpha_{ak}F}{RT}\eta_{s,k}\right) - \exp\left(-\frac{\alpha_{ck}F}{RT}\eta_{s,k}\right)\right] \qquad [70]$$

where the exchange-current density $i_{o,k}$ has the functional form

$$i_{o,k} = i_{o,k}^o \prod_j \left[\frac{C_j}{C_j^0}\right]^{\gamma_j} \qquad [71]$$

and the overpotential ($\eta_{s,k}$) driving force for the reaction is

$$\eta_{s,k} = \phi_1 - \phi_2 - U_k \qquad [72]$$

where

$$U_k = U_k^n + f(c_i, T) \qquad [73]$$

The potential variables ϕ_1 and ϕ_2 represent the potentials in the solid and solution phases, respectively, of either electrode. U_k is the thermodynamic open-circuit potential of the side reaction, and $i_{o,k}^o$, γ_j, α_{ak}, and α_{ck} are the kinetic parameters. The kinetic data will depend on the specific electrode materials in use and the composition of the electrolyte solution. U_k^n corresponds to the thermodynamic potential of reaction k under standard conditions.

An arbitrary number of side reactions can be included, each having its own overpotential defined above.[169] If the reactions are treated as occurring independently, the total current density at each electrode is a summation over the rates of all reactions

$$i = \sum_k i_k \qquad [74]$$

Using this treatment, depending on the value of the local potential and the thermodynamics of each reaction, cases can result where both anodic and cathodic reactions will occur on the same surface. This treatment will also predict the occurrence of corrosion or self-discharge processes

under open-circuit conditions. Obviously, the rates of all of the reactions are coupled through the potentials of each phase in the porous electrode and a numerical solution of the governing equations is necessary.

For many side reactions, the assumption of an irreversible reaction will hold, in which case the above rate expression can be simplified. A Tafel expression can be inserted in place of the Butler-Volmer equation

$$i_k = i_{o,k} \exp\left(\frac{\alpha_{ak} F}{RT} \eta_{s,k}\right) \quad [75]$$

For a side reaction obeying a Tafel equation, the value of the open-circuit potential becomes arbitrary because there is no longer a backward reaction. Thus, the only kinetic parameters of interest are the exchange-current density and Tafel slope (or transfer coefficient).

Once kinetic equations have been developed and rate expressions written, the number of species existing in the system and their relative importance can be assessed. Material balances can be written on each species existing in the system, although the concentrations of species involved in homogenous chemical reactions might be related through reaction equilibria.

The material balance for species i can be written in the form

$$\frac{\partial c_i}{\partial t} = -\nabla \cdot \underline{N}_i + R_i \quad [76]$$

where c_i and $\underline{N}_i$ are the concentration and molar flux of species i. The net rate of production of species i is given by R_i. This quantity applies to either bulk homogenous reactions or heterogeneous reactions if the latter are treated using a pseudohomogenous averaging approach. Under porous electrode theory, the rate of production of a given species can be related to the partial current densities of the electrochemical reactions according to[169]

$$R_i = -\sum_k a_k \frac{s_{i,k}}{n_k F} i_k \quad [77]$$

where a_k is the specific interfacial area per unit volume of electrode. If the electrochemical reaction is localized onto a particular surface, such as the current collector, the generation of material can be included in a boundary condition. Different approximations will be valid depending on the phase of the species (solid, liquid, gases) and the concentrations present. In many cases, the rate of a side reaction will be low enough or the quantity of a species generated small enough that a material balance can be neglected entirely.

Often transport processes in the cell are described using concentrated solution theory which accounts for interactions between each pair of species.[169] With a larger number of species present due to side reactions, simplifications may be made to this rigorous treatment to reduce the number of transport properties required in the model. For example, the electrolyte solution might be treated as composed of a primary solvent, a single salt, and an arbitrary number of solution-phase pseudo-dilute species. Interactions between the primary solvent and salt are treated rigorously as a binary electrolyte system, while the dilute species are treated as interacting with the primary solvent only. This simplified treatment generates $(3 + n)$ transport properties or D_{ij}'s where n is the number of dilute species rather than the $(3 + n)(2 + n)/2$ required in the more rigorous treatment. Neglected in this treatment are interactions between the various dilute species and interactions of dilute species with the salt.

Under these simplifications, the flux of a dilute nonionic component might be written simply as

$$\underline{N}_i = -D_{0i} \nabla c_i \quad [78]$$

where D_{0i} is an interaction parameter or diffusion coefficient representing motion of species i through the solvent. The flux of a dilute ionic component is composed of the above diffusive flux as well as a migration components

$$\underline{N}_i = -D_{0i} \nabla c_i - z_i \frac{D_{0i}}{RT} F c_i \nabla \phi \quad [79]$$

If the concentration of a dilute ionic component is low enough, migration can be neglected entirely because the primary salt will act as a supporting electrolyte. In both of the above expressions, convective fluxes are neglected which is usually a good approximation. These flux expressions are substituted into the material balance above (Eq. 76) to provide an equation for the concentration of a dilute species as a function of time and position across the cell. Initial and boundary conditions are needed to complete the problem.

The phase of a given species is an important consideration in determining the level of sophistication required in the model. For example, gaseous species might be treated as existing purely in a vapor space above the cell, and their concentrations might be assumed uniform because of fast transport of gas-phase species. Under these assumptions, the pressure developed inside the cell could be assessed (assuming the system is at constant volume) and the relative partial pressures of each species determined. In other cases, the solubility of gases in the electrolyte may be an important factor in cell performance or self-discharge processes, in which case these assumptions would not be made. The three phases (solid, solution, and gas) can be treated as superimposed continuous phases without regard to the geometric details of the pore structure using porous electrode theory.[169,170]

Solid-phase species with low solubility might be treated as localized, such as with the precipitation of salts in previous battery modeling literature.[172-176] Reactive intermediates, such as radical species resulting from solvent oxidation or reduction processes, are often treated using the pseudo-steady-state approximation, wherein the net rate of formation of the species is assumed to be zero.[177] Further consequences of these assumptions will be discussed in the remainder of this section.

Film growth.—Side reactions that lead to growth of a film on the surface of the electrode particles are seen in several instances within the lithium-ion battery. Passivation of the carbon-based negative electrode with associated film or SEI layer formation is a standard process in all cells. Abuse conditions such as overcharge can lead to film formation from the deposition of metallic lithium onto the negative electrode. Any lithium metal formed in the cell will probably undergo secondary reactions leading to more thick reaction product layers or secondary films. Other side reactions can also lead indirectly to film formation because of the formation of products with low solubility in the nonaqueous solvents.

We start by discussing film formation due to overcharge of the negative electrode and deposition of metallic lithium because this process is possible in all lithium-ion batteries in theory and presents an important safety concern with commercial cells. A number of different approximations can be used to include the lithium metal deposition side reaction in lithium-ion battery models. For this reason, the detail of a model is driven primarily by its intended usage, with models having more predictive power needing a greater level of detail. Before decisions can be made on the sophistication needed, overcharge experimental data for lithium-ion cells using coke and graphite as negative electrodes are needed. Based on these data, the effects of overcharge on the discharge and cycle life of the battery can be assessed, and the phenomena that must be incorporated into models determined. Also, kinetic data for the lithium deposition reaction are needed under the appropriate conditions.

Because the lithium deposition reaction is a facile process under many conditions, the surface overpotential will be low and the reaction can be described adequately using the linear approximation to the Butler-Volmer equation

$$i_k = i_{o,k} \frac{(\alpha_a + \alpha_c)F}{RT} \eta_s \quad [80]$$

For solids such as metallic lithium, the flux will be zero to a very good approximation. By integrating the material balance over the volume of the negative electrode, the rate of the side reaction can be related to the growth of a film on the surface of the electrode particles

$$\frac{\partial \delta}{\partial t} = \frac{i_k M}{L_- a \rho F} \quad [81]$$

where δ is the film thickness composed of solid lithium and other lithium products, and L_- represents the thickness of the negative electrode.

This film thickness, along with assumed properties for the film such as conductivity and dielectric constant, can be incorporated into a battery model to predict the impact on discharge performance or electrochemical impedance data. A similar approach was taken by Pollard to treat precipitation of salt films in electrochemical cells.[175] As the film thickens dynamically during simulation of the cell charge and discharge, the interfacial resistance will increase and the current distribution in the electrodes will change. Also, the capacity balance in the cell is modified due to the side reaction current density. Other effects can then be incorporated such as porosity changes in the electrode and secondary side reactions with the deposited lithium.

Another side reaction of general interest in lithium-ion batteries is passive film formation on the negative electrode during the initial cycling or formation period. Modeling passive film formation is similar to the modeling of lithium deposition during overcharge conditions. However, the reduction reactions taking place which lead to the deposition of solid products are much less well understood, larger in number, and varied in their nature depending on the composition of the electrolyte solution as seen in an earlier section. For these reasons, a great simplification might be made where the passivation process is treated as the consumption of solvent and lithium ions to form a single homogeneous product such as lithium carbonate. The passivation process at the electrode/electrolyte interface can be modeled to allow the film thickness and other relevant properties to be tracked during cycling. Other intermediate species formed such as radicals could be either neglected completely or treated in a simplified manner (for example, these might be included to track the rate of self-discharge). By following the rate of solvent, lithium ion, and electron consumption by the passivation process, the important effects of the side reaction on the capacity balance in the cell can still be assessed.

Under the assumptions given above, the film is modeled as a one-dimensional layer having a time-dependent film thickness. The film thickness is calculated from the partial current density of the reduction side reaction. Because the exact nature of the side reaction is either not known or is being simplified greatly, the rate expression used would probably be obtained by empirical fits to experimental data such as charge and discharge curves during the formation period. The film thickness calculated from the model is related to a film resistance and capacitance using assumed physical properties. Because the resistance of the film changes with time, an increase in interfacial resistance and a capacity loss in the cell will result. Assuming that the rate-limiting step in the charge-transfer process is bulk migration of lithium through this passive layer as stated earlier, then the treatment of the film as a pure resistor is justified. In other cases, the finite rate of the charge-transfer process at either interface may also be an important consideration. Finally, if the film has some porosity or if it is not a pure cation conductor, then diffusion limitations inside the film might also be included.[172]

Electrolyte decomposition reactions.—A large number of different solvent and salt combinations are used in lithium-ion batteries. Because of the complexity of the mechanisms of salt and solvent oxidation and reduction reactions, it is not possible at present to create a general model that can treat all possible systems. Future modeling work in this area will almost certainly be confined to specific and well-studied systems. The modeling of electrolyte decomposition reactions is not difficult mathematically, but for complicated multistep mechanisms, the number of equations and unknowns make the solution procedure computationally demanding. Kinetic data for each reaction and transport property data for each species are in theory needed. It should be possible to treat these systems by making use of standard approaches such as the pseudo-steady-state or rate-limiting-step approximate methods.[177]

A rigorous treatment of side reactions involving the solvent and salt species in lithium-ion cells would require substantial amounts of fundamental data on the rates of these processes so that information such as rate-limiting steps can be assessed. Fortunately, for the practical purpose of treating side reactions in battery modeling and predicting their consequences to cell performance, this level of detail is probably unnecessary, and advances in the understanding of these processes can be made using the present state of knowledge in the literature. Side reactions involving both oxidation and reduction of components of the electrolyte solution are lumped together in this section because similar issues exist in modeling both situations, such as the loss of solvent or salt from the system, formation of product species which may take part in secondary processes or reactions, and perturbation of the cell's capacity balance.

In many current lithium-ion battery models, the open-circuit potential of the positive electrode is forced to infinity as the value of y reaches its minimum value (e.g., $U \rightarrow \infty$ as $y \rightarrow 0.4$ for Li_yCoO_2) and no side reactions involving electrolyte oxidation are considered. Applying this condition to the open-circuit potential for the insertion electrode stops the insertion process at the desired stoichiometry in an artificial manner by forcing the electrode polarization to infinity. Side reactions (both chemical and electrochemical) could be included in a battery model as secondary processes that proceed in parallel to the main reaction with their own separate kinetic expressions. The electrochemical side reactions depend on the local electrode potential and are often treated adequately using Tafel equations due to the irreversible nature of many of these processes.[35] Chemically or thermally induced degradation processes do not depend on electrode potential and might be more important under conditions of abuse.

The presence of these side reactions can have a number of dramatic consequences in a battery model. By tracking the rates of the oxidation or reduction processes occurring as side reactions, the actual lithium stoichiometry in the two insertion electrodes is predictable even during abuse conditions. This allows capacity fading to be predicted as well as the potential hazards associated with accumulated loss of capacity in one electrode. In many cases, the loss of salt or solvent from the cell will represent a very small fraction of the total electrolyte, and this effect on the cell's performance might be neglected entirely. However, over long-term cycling of the cell, it is possible that the accumulated loss of electrolyte from the system will begin to manifest itself in losses of rate capability or cell capacity. Products formed in the side reactions can also be monitored and their role in secondary processes such as self-discharge followed. These products might be solution phase, gaseous, or solid depending on the nature of the side reaction, and in each case different approximations are warranted as discussed earlier.

In some cases, the active electrode material itself may take part in the side reaction. For example, the acid-induced delithiation and dissolution of the manganese oxide spinel material is a case where solvent oxidation or salt hydrolysis processes lead to the formation of products (protons) that participate in secondary reactions with the electrode material. Often these processes will lead to formation of electrochemically inactive products either due to blockage of the electrode particle surface due to precip-

itation of solid-phase species or because of conversion to materials with either limited reversibility or no lithium insertion capacity in the voltage range of interest.

Modeling these processes requires a mass balance for each species involved in the side reactions, especially those related to consumption of active materials and formation of inert products. A more simplistic method of accounting for the formation of inert or nonelectrochemically active metal oxide compounds is to adjust the volume fraction of active material as the side reaction proceeds, increasing the volume of inert filler in proportion to the rate of active material consumption. For example, by tracking the production of protons inside the cell under abuse conditions (such as solvent oxidation), the rate of electrode dissolution and conversion to nonactive materials can also be followed. These nonactive materials could be treated as uniformly distributed throughout the composite electrode similar to the standard treatment of polymer binders and carbon-black additives under porous electrode theory.

Corrosion and dissolution processes.—Additional ionic species can make their way into the cell due to the processes of electrode dissolution and current collector corrosion. Cationic species other than lithium can create problems for cell performance because they are more easily reducible than lithium ions and will generally end up depositing on the negative electrode during charging conditions. In the worst case, these processes lead to dendritic growth through the separator and short circuit of the cell. The presence of deposited manganese and cobalt have been mentioned in the literature,[52,125,131,139,142] and corrosion of current collector materials such as copper and aluminum is also well documented.[119-121] Modeling these phenomena appears challenging due to our limited understanding of the fundamental processes occurring and the fate of metallic impurities inside the nonaqueous environment of the cell (other than their eventual likely fate at the negative electrode).

For example, it would be useful to predict the onset of copper dissolution at the negative electrode under overdischarge conditions. This might allow more optimum design of cells to limit the maximum negative electrode potential and prevent significant loss of copper. Unfortunately, the copper dissolution-deposition voltage is difficult to predict because very little data are available for nonaqueous systems. For any given nonaqueous electrolyte system, the thermodynamic open-circuit potential for copper dissolution must be assessed experimentally. If these data were known or assumed, the copper dissolution reaction could be modeled in a manner similar to the treatment of lithium deposition during negative-electrode overcharge by using a Butler-Volmer-type rate equation and a material balance on solution-phase copper species. However, the growth of dendrites leading to cell short circuit is more difficult to predict because this is a function of deposition morphology.

The related topic of electrode dissolution in $LiMn_2O_4$-based cells can be included in battery models by adding the acid-assisted dissolution mechanism discussed earlier as a side reaction. Equation 59 occurs on the surface of the positive electrode, $LiPF_6$ hydrolysis is a homogenous chemical reaction, and H_2 evolution occurs at the surface of the negative electrode. Note that these processes are potentially autocatalytic as water generated by the dissolution of the lithium manganese oxide spinel can create more protons from hydrolysis of the salt. These reactions can be included in a cell model by writing material balances for each species, although a number of simplifications are sure to be warranted. The rate equation (Butler-Volmer expression for electrochemical reactions) for each reaction could be written in the same manner as shown previously (Eq. 70). Positive active material is lost when electrode dissolution occurs leading to capacity loss. Also, dissolved manganese is reduced at the negative electrode and blocks pores or surface area again leading to capacity loss.

Self-discharge processes.—Although self-discharge is an important phenomena for practical commercial cells, it has received relatively little attention in the battery modeling literature. However, the modeling of self-discharge processes is straightforward once a full-cell-sandwich battery model exists and once the necessary side reactions have been incorporated into the model. Self-discharge processes can be separated into those involving a single electrode such as the coupled electrolyte decomposition and lithium insertion-deinsertion reactions discussed earlier, and those that involve interactions between the two electrodes such as redox processes and short-circuiting.

Self-discharge processes involving a single electrode can be treated by simply adding the kinetics for the electrolyte decomposition reaction as well as Eq. 74 to the overall mathematical model. For example, self-discharge of a high-voltage positive electrode would be modeled by including the oxidation of solvent species such as the carbonates using a Tafel rate expression.[35] Because of the behavior of the Tafel equation, the solvent oxidation process would occur at all voltages but would increase dramatically at higher voltages dependent on the values used for the exchange-current density and transfer coefficient for the oxidation reaction. When the current is interrupted in a model of this kind, rather than attaining a constant voltage, the cell voltage will decrease spontaneously as lithium intercalation into the positive electrode is balanced against the solvent oxidation process.

Other self-discharge mechanisms could also be included in a macroscopic battery model without much trouble. Leakage currents are included in modeling by carrying out the constant resistance discharge of the cell under otherwise open-circuit conditions. It might be possible to measure the proper value of resistance to use for the discharge or this value might be fit against experimental self-discharge data. Redox-shuttle-type self-discharge mechanisms require a source for the redox species, such as a solvent decomposition reaction, as well as a material balance on the species in question to predict its transport rate across the cell and concentration (both of which impact the self-discharge rate). Self-discharge processes have been verified experimentally in the literature described earlier, but more experimental data will be needed to validate model predictions using well-characterized systems.

Acknowledgments

The authors acknowledge the financial support from the Office of Research and Department of the United States Central Intelligence Agency for this project under contract no. 93-F148100-100. The authors also acknowledge useful discussions on capacity fade mechanisms with Dr. A. S. Gozdz of Bellcore.

Manuscript submitted November 18, 1997; revised manuscript received April 17, 1998.

The University of South Carolina assisted in meeting the publication costs of this article.

LIST OF SYMBOLS

a_k	specific interfacial area per unit volume of electrode, cm^{-1}
c_i	concentration of species i, mol/cm^3
C	theoretical coulombic capacity of insertion material based on discharged state, mAh/g
C_{irr}	excess capacity in negative electrode, mAh/g
El	electrolyte constituent
F	Faraday's constant, 96487 C/equiv
i	current density, A/cm^2
$i_{o,k}$	exchange current density of reaction k, A/cm^2
m	mass of active material in composite electrode, g
M	molecular weight, g/mol
L	thickness of electrode, μm
n	number of electrons transferred in electrochemical reactions
N_i	molar flux of species i, mol/cm^2 s
R	ideal gas constant, 8.314 J/ mol K
R_i	rate of generation of species i, mol/cm^3 s
s_i	stoichiometric coefficient of species i
t	time, s

T temperature, K
U open-circuit potential, V
x stoichiometric coefficient of negative electrode
y stoichiometric coefficient of positive electrode

Greek

α transfer coefficient
γ reaction order of species i or mass ratio of electrodes
δ thickness, cm
ϵ volume fraction of active material in electrode
ρ density, g/cm^3
η surface overpotential, V
ϕ electric potential, V

Subscripts

0 with respect to initial conditions
1 solid matrix
2 solution phase
+ positive electrode
− negative electrode
a anode
c cathode
k reaction number
s separator

Superscripts

θ standard cell potential

REFERENCES

1. B. Scrosati, *J. Electrochem. Soc.*, **139,** 10 (1992).
2. S. Megahed and B. Scrosati, *Electrochem. Soc. Interface*, **4**(4), 34 (1995).
3. T. Nagaura, *Prog. Batteries Battery Mater.*, **10,** 218 (1991).
4. K. G. McColl, *J. Power Sources*, **48,** 29 (1994).
5. D. Linden, *Handbook of Batteries and Fuel Cells*, 1st ed., McGraw-Hill Book Company, New York (1984).
6. K. M. Abraham, *Electrochim. Acta*, **38,** 1233 (1993).
7. K. Brandt, *Solid State Ionics*, **69,** 173 (1994).
8. K. Sekai, H. Azuma, A. Omaru, S. Fujita, H. Imoto, T. Endo, K. Yamaura, and Y. Nishi, *J. Power Sources*, **43-44,** 241 (1993).
9. K. Ozawa, *Solid State Ionics*, **69,** 212 (1994).
10. B. A. Johnson and R. E. White, *J. Power Sources*, **70/1,** 48 (1998).
11. S. Yoda, *J. Power Sources*, **68,** 3 (1997).
12. B. C. Knutz, K. West, B. Z.-Christiansen, and S. Atlung, *J. Power Sources*, **43-44,** 733 (1993).
13. K. West, T. Jacobsen, and S. Atlung, *J. Electrochem. Soc.*, **129,** 1480 (1982).
14. S. Atlung, K. West, and T. Jacobsen, *J. Electrochem. Soc.*, **126,** 1311 (1979).
15. S. Atlung, B. Z.-Christiansen, K. West, and T. Jacobsen, *J. Electrochem. Soc.*, **131,** 1200 (1984).
16. Z. Mao and R. E. White, *J. Power Sources*, **43-44,** 181 (1993).
17. R. M. Spotnitz, D. Zuckerbrod, S. L. Johnson, J. T. Lundquist, and R. E. White, in *Proceedings of the Symposium on Modeling of Batteries and Fuel Cells*, R. E. White, M. W. Verbrugge, and J. F. Stockel, Editors, PV 91-10, p. 88, The Electrochemical Society, Proceedings Series, Pennington, NJ (1991).
18. M. Doyle, T. F. Fuller, and J. Newman, *J. Electrochem. Soc.*, **140,** 1527 (1993).
19. T. F. Fuller, M. Doyle, and J. Newman, *J. Electrochem. Soc.*, **141,** 1 (1994).
20. M. Doyle, Ph.D Thesis, University of California, Berkeley, CA (1995).
21. T. F. Fuller, M. Doyle, and J. Newman, *J. Electrochem. Soc.*, **141,** 982 (1994).
22. M. Doyle, J. Newman, A. S. Gozdz, C. N. Schmutz, and J. M. Tarascon, *J. Electrochem. Soc.*, **143,** 1890 (1996).
23. M. Doyle, J. Newman, and J. Reimers, *J. Power Sources*, **52,** 211 (1994).
24. M. Doyle and J. Newman, *J. Power Sources*, **54,** 46 (1995).
25. Y. Chen and J. W. Evans, *J. Electrochem Soc.*, **140,** 1833 (1993).
26. Y. Chen and J. W. Evans, *J. Electrochem Soc.*, **141,** 2947 (1994).
27. Y. Chen and J. W. Evans, *J. Electrochem Soc.*, **143,** 2708 (1996).
28. C. R. Pals and J. Newman, *J. Electrochem Soc.*, **142,** 3274 (1995).
29. C. R. Pals and J. Newman, *J. Electrochem Soc.*, **142,** 3282 (1995).
30. M. W. Verbrugge and B. J. Koch, *J. Electrochem. Soc.*, **143,** 24 (1996).
31. M. W. Verbrugge and B. J. Koch, *J. Electrochem. Soc.*, **143,** 600 (1996).
32. S. R. Narayanan, S. Surampudi, A. I. Attia, and C. P. Bankston, *J. Electrochem. Soc.*, **138,** 8 (1991).
33. R. Darling and J. Newman, *J. Electrochem. Soc.*, **144,** 4201 (1997).
34. G. Nagarajan, J. W. VanZee, and R. M. Spotnitz, *J. Electrochem. Soc.*, **145,** 771 (1998).
35. R. Darling and J. Newman, *J. Electrochem. Soc.*, **145,** 990 (1998).
36. M. Armand, *Solid State Ionics*, **9&10,** 745 (1983).
37. J. M. Tarascon and D. Guyomard, *Electrochim. Acta*, **38,** 1221 (1993).
38. D. Guyomard and J. M. Tarascon, *Solid State Ionics*, **69,** 222 (1994).
39. R. Pollard and J. Newman, *J. Electrochem Soc.*, **128,** 491 (1981).
40. A. B. Yu, R. P. Zou, and N. Standish, *Ind. Eng. Chem. Res.*, **35,** 3730 (1996).
41. D. Guyomard and J. M. Tarascon, *J. Electrochem. Soc.*, **139,** 4 (1992).
42. R. Fong, U. von Sacken, and J. R. Dahn, *J. Electrochem. Soc.*, **137,** 2009 (1990).
43. D. Fauteux and R. Kosbang, *J. Appl. Electrochem.*, **22,** 1 (1992).
44. T. Zheng, Y. Liu, E. W. Fuller, S. Tseng, U. von Sacken, and J. R. Dahn, *J. Electrochem. Soc.*, **142,** 2581 (1995).
45. W. Xing and J. R. Dahn, *J. Electrochem. Soc.*, **144,** 1195 (1997).
46. J. R. Dahn, T. Zheng, Y. Liu, and J. S. Xue, *Science*, **270,** 590 (1995).
47. J. M. Tarascon and D. Guyomard, *J. Electrochem. Soc.*, **138,** 2865 (1991).
48. J. M. Tarascon and D. Guyomard, *J. Power Sources*, **43-44,** 689 (1993).
49. D. Peramunage, K. M. Abraham, and E. B. Willstaedt, in *13th Proceedings of the Annual Battery Conference on Applications and Advances*, Long Beach, CA, p. 107, Jan 13-16, 1998.
50. E. Peled, Abstract 72, p. 114, The Electrochemical Society Meeting Abstracts, Vol. 94-2, Miami Beach, FL, Oct 9-14, 1994.
51. E. Peled, in *Lithium Batteries*, J. P. Gabano, Editor, Academic Press New York (1983).
52. J. R. Dahn, E. W. Fuller, M. Obravae, and U. von Sacken, *Solid State Ionics*, **69,** 265 (1994).
53. A. S. Gozdz and R. K. Jaworski, Abstract 43, p. 52, The Electrochemical Society Meeting Abstracts, Vol. 96-1, Los Angeles, CA, May 5-10, 1996.
54. Y. Ein-Eli, B. Markovsky, D. Aurbach, Y. Carmeli, H. Yamin, and S. Luski, *Electrochim. Acta*, **39,** 2559 (1994).
55. R. J. Staniewicz, in *13th Proceedings of The International Seminar on Primary and Secondary Battery Technology and Applications*, Boca Raton, FL, March 4-7, 1996.
56. F. A. Cotton and G. Wilkinson, *Advanced Inorganic Chemistry*, 3rd ed., John Wiley & Sons, Inc., New York (1993).
57. G. A. Nazri, A. Rougier, and K. F. Kia, *Mater. Res. Soc. Symp. Proc.*, **453**, 635 (1997).
58. M. Hasegawa, B. Yasuhiko, M. Toshihide, and T. Yoshinori, U.S. Pat. 5,631,105 (1997).
59. Y. Junichi, O. Kazuhiro, and N. Yoshiaki, U.S. Pat. 5,626,635 (1997).
60. C. Delmas, *Solid State Ionics*, **53-56,** 370 (1992).
61. W. Li and J. C. Currie, *J. Electrochem. Soc.*, **144,** 2773 (1997).
62. M. M. Thackeray, M. F. Mansuetto, D. W. Dees, and D. R. Vissers, *Mater. Res. Bull.*, **31,** 133 (1996).
63. Y. Gao and J. R. Dahn, *Solid State Ionics*, **84,** 33 (1996).
64. J. M. Tarascon and D. Guyomard, *Solid State Ionics*, **69,** 293 (1994).
65. S. A. Campbell, C. Bowes, and R. S. McMillan, *J. Electroanal. Chem.*, **284,** 195 (1990).
66. K. Kanamura, S. Toriyama, S. Shiraishi, and Z. Takehara, *J. Electrochem. Soc.*, **142,** 1383 (1995).
67. A. M. Christie and C. A. Vincent, *J. Appl. Electrochem.*, **26,** 255 (1996).

68. F. Ossola, G. Pistoia, R. Seeber, and P. Ugo, *Electrochim. Acta,* **33,** 47 (1988).
69. P. Novak, P. A. Christensen, T. Iwasita, and W. Vielstich, *J. Electroanal. Chem.,* **263,** 37 (1989).
70. E. Cattaneo and J. Ruch, *J. Power Sources,* **43-44,** 341 (1993).
71. G. Eggert, and J. Heitbaum, *Electrochim. Acta,* **31,** 1443 (1986).
72. K. Kanamura, H. Takezawa, S. Shiraishi, and Z. Takehara, *J. Electrochem. Soc.,* **144,** 1900 (1997).
73. K. Kanamura, S. Toriyama, S. Shiraishi, and Z. Takehara, *J. Electrochem. Soc.,* **143,** 2548 (1996).
74. S. Oishi, T. Abe, T. Nagaura, and M. Watanabe, U.S. Pat. 4,943,497 (1990).
75. M. N. Golovin, D. P. Wilkinson, J. T. Dudley, D. Holonko, and S. Woo, *J. Electrochem. Soc.,* **139,** 5 (1992).
76. T. J. Richardson and P. N. Ross, Jr., *J. Electrochem. Soc.,* **143,** 3992 (1996).
77. K. M. Abraham, D. M. Pasquariello, and E. B. Willstaedt, in *Proceedings of the 33rd Power Sources Symposium,* Cherry Hill, NJ, June 13-16, p. 38, The Electrochemical Society, Inc. (1988).
78. W. K. Behl and D. T. Chin, *J. Electrochem. Soc.,* **135,** 18 (1988).
79. W. K. Behl and D. T. Chin, *J. Electrochem. Soc.,* **135,** 21 (1988).
80. K. J. Hanson and C. W. Tobias, *J. Electrochem. Soc.,* **134,** 2204 (1987).
81. K. J. Hanson, M. J. Matlosz, C. W. Tobias, and J. Newman, *J. Electrochem. Soc.,* **134,** 2210 (1987).
82. K. Ozawa, *Solid State Ionics,* **69,** 212 (1994).
83. F. C. Laman, M. A. Gee, and J. Denovan, *J. Electrochem. Soc.,* **140,** L51 (1993).
84. J. T. Lundquist, C. B. Lundsager, N. I. Palmer, and H. J. Troffkin, U.S. Pat. 4,650,730 (1987).
85. J. T. Lundquist, C. B. Lundsager, N. I. Palmer, and H. J. Troffkin, U.S. Pat. 4,731,304 (1988).
86. H. T. Taskier, S. M. Mullins, E. A. Langford, and R. J. Fleming, U.S. Pat. 4,973,532 (1990).
87. A. Yoshino, K. Nakanishi, and A. Ono, Jpn Pat. Appl. Tokugan Hei 1-338559 (1989).
88. R. Spotnitz and M. Ferebree, Abstract 132, p. 179, The Electrochemical Society Meeting Abstracts, Vol. 96-2, San Antonio, TX, Oct 6-11, 1996.
89. U. von Sacken, Paper presented at *POWER '97,* 5th International Conference on Power Requirements for Mobile Computing and Wireless Communications, Santa Clara, CA, Oct 12-15, 1997.
90. D. Guyomard and J. M. Tarascon, *J. Power Sources,* **54,** 92 (1995).
91. D. Aurbach, Y. Ein-Eli, O. Chusid, Y. Carmeli, M. Babai, and H. Yamin, *J. Electrochem. Soc.,* **141,** 603 (1994).
92. A. N. Dey and B. P. Sullivan, *J. Electrochem. Soc.,* **117,** 222 (1970).
93. O. Chusid, Y. Ein-Eli, and D. Aurbach, *J. Power Sources,* **43-44,** 47 (1993).
94. Y. Matsumura, S. Wang, and J. Mondori, *J. Electrochem. Soc.,* **142,** 2914 (1995).
95. Z. X. Shu, R. S. McMillan, and J. J. Murray, *J. Electrochem. Soc.,* **140,** 922 (1993).
96. A. C. Chu, J. Y. Josefowicz, and G. C. Farrington, *J. Electrochem. Soc.,* **144,** 4161 (1997).
97. D. Aurbach, M. L. Daroux, P. W. Faguy, and E. Yeager, *J. Electrochem. Soc.,* **134,** 1611 (1987).
98. D. Bartow, E. Peled, and L. Burstein, Abstract 835, p. 1028, The Electrochemical Society Meeting Abstracts, Vol 96-2, San Antonio, TX, Oct 6-11, 1996.
99. Y. Ein-Eli, S. R. Thomas, and V. R. Koch, *J. Electrochem. Soc,* **144,** 1159 (1997).
100. Y. Ein-Eli, S. F. McDevitt, D. Aurbach, B. Markovsky, and A. Schechter, *J. Electrochem. Soc.,* **144,** L180 (1997).
101. K. Yokoyama, A. Hiwara, S. Fujita, and A. Omaru, U.S. Pat. 5,633,099 (1997).
102. Z. X. Shu, R. S. McMillan and J. J. Murray, U.S. Pat. 5,571,635 (1996).
103. Z. X. Shu, R. S. McMillan, J. J. Murray, and I. J. Davidson, *J. Electrochem. Soc.,* **142,** L161 (1995).
104. D. Aurbach, B. Markovsky, A Shechter, and Y. Ein-Eli, *J. Electrochem. Soc.,* **143,** 3809 (1996).
105. D. Aurbach, B. Markovsky, A. Shechter, and Y. Ein-Eli, *J. Electrochem. Soc.,* **143,** 3809 (1997).
106. D. Aurbach, Y. Ein-Eli, B. Markovsky, A. Zaban, A. Schechter, S. Luski, Y. Carmeli, and H. Yamin, in *Rechargeable Lithium and Lithium-Ion Batteries,* S. Megahed, B. M. Barnett, and L. Xie, Editors, PV 94-28, p. 26, The Electrochemical Society Proceedings Series, Pennington, NJ (1994).
107. R. Imhof and P. Novak, Abstract 125, p. 139, The Electrochemical Society Meeting Abstracts. Vol. 97-2, Paris, France, Aug 31-Sept 5, 1997.
108. M. Jean, A. Chausse, and R. Messina, Abstract 146, p. 169, The Electrochemical Society Meeting Abstracts, Vol. 97-2, Paris, France, Aug 31-Sept 5, 1997.
109. B. Simon, J. P. Boeuve, and M. Broussely, *J. Power Sources,* **43-44,** 65 (1993).
110. G. Pistoia, D. Zane, and Y. Zhang, *J. Electrochem. Soc.,* **142,** 2551 (1995).
111. G. Pistoia, A. Antonini, R. Rosati and D. Zane, *Electrochim. Acta,* **41,** 2683 (1996).
112. E. Peled, D. Golodnitsky, G. Ardel, C. Menachem, D. Bar Tow, and V. Eshkenazy, *Mater. Res. Soc. Symp. Proc.,* **393,** 209 (1995).
113. E. Peled, *J. Power Sources,* **9,** 253 (1983).
114. E. Peled, D. Golodnitsky, G. Ardel, and V. Eshkenazy, *Electrochim. Acta,* **40,** 2197 (1995).
115. A. Meitav and E. Peled, *J. Electrochem. Soc.,* **128,** 825 (1981).
116. E. Peled and H. Straze, *J. Electrochem. Soc.,* **124,** 1030 (1977).
117. U. von Sacken, E. Nodwell, A. Sundher, and J. R. Dahn, *Solid State Ionics,* **69,** 284 (1994).
118. M. Garreau, J. Thevenin, and B. Milandou, in *Lithium Batteries,* A. N. Dey, Editor, PV 84-1, p. 28, The Electrochemical Society Proceedings Series, Pennington, NJ (1984).
119. J. W. Braithwaite, A. Gonzales, S. L. Lucero, D. E. Peebles, J. A. Ohlhausen, W. R. Ciesalk, and G. Nagasubramanian, Sandia National Laboratories Report, SAND97-0507 (1997).
120. J. Braithwaite, G. Nagasubramanian, S. Lucero, and W. Cieslak, Abstract 64, p. 85, The Electrochemical Society Meeting Abstracts, Vol. 96-2, San Antonio, TX, Oct 6-11, 1996.
121. G. Pistoia, A. Antonini, R. Rosati, and C. Bellitto, Abstract 213, p. 257, The Electrochemical Society Meeting Abstracts, Vol. 97-2, Paris, France, Aug 31-Sept 5, 1997.
122. Y. Chen, L. Song, T. M. Devine, and J. W. Evans, Two papers presented at Advanced Non-Aqueous Battery Technology Research and Development Workshop, p. 49, Oct 15-17, 1997.
123. *IUPAC Chemical Data Series-No.22, Stability Constants of Metal-Ion Complexes,* Part B, *Organic Ligands,* Compiled by Douglas D. Perrin, Pergamon Press, New York (1979).
124. G. G. Amatucci, Unpublished results.
125. M. M. Thackeray, *J. Electrochem. Soc.,* **142,** 2558 (1995).
126. M. M. Thackeray, *J. Electrochem. Soc.,* **144,** L100 (1997).
127. J. M. Tarascon, W. R. McKinnon, F. Coowar, T. N. Bowmer, G. Amatucci, and D. Guyomard, *J. Electrochem. Soc.,* **141,** 1421 (1994).
128. R. J. Gummow, A. de Kock, and M. M. Thackeray, *Solid State Ionics,* **69,** 59 (1994).
129. S. J. Wen, T. J. Richardson, L. Ma, K. A. Striebel, P. N. Ross, Jr., and E. J. Cairns, *J. Electrochem. Soc.,* **143,** L136 (1996).
130. Y. Xia, Y. Zhou, and M. Yoshio, *J. Electrochem. Soc.,* **144,** 2593 (1997).
131. A. Blyr, C. Sigala, G. Amatucci, D. Guyomard, Y. Chabre, and J-M. Tarascon, *J. Electrochem. Soc.,* **145,** 194 (1998).
132. O. Schilling and J. R. Dahn, *J. Electrochem. Soc.,* **145,** 569 (1998).
133. Y. Shao-Horn, Y. Ein-Eli, A. D. Robertson, W. F. Averill, S. A. Hackney, and W. F. Howard, Jr., *J. Electrochem. Soc.,* **145,** 16 (1998).
134. J. C. Hunter, *J. Solid State Chem.,* **39,** 142 (1981).
135. S. Lu, W. F. Averill, A. D. Robertson, and W. F. Howard, Jr., in *13th Proceedings of The International Seminar on Primary and Secondary Battery Technology and Applications,* Boca Raton, FL, March 4-7, 1996.

136. G. G. Amatucci, I. Plitz, D. Larcher, J. Shelburne, and J. M. Tarascon, The 14th International Seminar on Primary and Secondary Batteries, Fort Lauderdale, FL, March 10-13, 1997.
137. J. M. Tarascon, F. Coowar, G. G. Amatucci, F. K. Shokoohi, and D. G. Guyomard, *J. Power Sources*, **54,** 103 (1997).
138. A. S. Gozdz, Private communication.
139. D. H. Jang, Y. J. Shin, and S. M. Oh, *J. Electrochem. Soc.*, **143,** 2204 (1996).
140. D. H. Jang and S. M. Oh, *J. Electrochem. Soc.*, **144,** 3342 (1997).
141. A. D. Robertson, S. H. Lu, and W. F. Howard, *J. Electrochem. Soc.*, **144,** 10 (1997).
142. G. G. Amatucci, J. M. Tarascon, and L. C. Klien, *Solid State Ionics*, **83,** 167 (1996).
143. S. Tobishima, K. Hayashi, K. Saito, T. Shodai, and J. Yamaki, *Electrochim. Acta*, **42,** 119 (1997).
144. T. Ohzuku, M. Kitagawa, and T. Hirai, *J. Electrochem. Soc.*, **137,** 769 (1990).
145. Y. Xia and M. Yoshio, *J. Electrochem. Soc.*, **143,** 825 (1996).
146. E. J. Cairns, C. R. Home, B. J. R. Weiss, M. M. Grush, and S. P. Cramer, in *Proceedings of 2nd Symposium on New Materials for Fuel Cell and Modern Battery Systems*, July 1997.
147. A. Yamada, K. Miura, K. Hinokuma, and M. Tanaka, *J. Electrochem. Soc.*, **142,** 2149 (1995).
148. T. Ohzuku, J. Kato, S. Keijiro, and T. Hirai, *J. Electrochem. Soc.*, **138,** 2556 (1991).
149. L. Guohua, H. Ikuta, T. Uchida, and M. Wakihara, *J. Electrochem. Soc.*, **143,** 178 (1996).
150. P. Arora, G. Zheng, B. N. Popov, and R. E. White, Abstract 90, p. 104, The Electrochemical Society Meetings Abstracts, Vol. 97-1, Montreal, Quebec, Canada, May 4-9, 1997.
151. P. Arora, B. N. Popov, and R. E. White, *J. Electrochem. Soc.*, **145,** 807 (1998).
152. G. G. Amatucci, I. Plitz, D. Larcher, A. Blyr, J. Shelburne, and J. M. Tarascon, Abstract 84, p. 97, The Electrochemical Society Meeting Abstracts, Vol. 97-1, Montreal, Quebec, Canada, May 4-9, 1997.
153. G. G. Amatucci, I. Plitz, J. Shelburne, and J. M. Tarascon, Abstract 85, p. 98, The Electrochemical Society Meeting Abstracts, Vol. 97-1, Montreal, Quebec, Canada, May 4-9, 1997.
154. P. G. Bruce, *Chem. Commun.*, 1817 (1997).
155. Y. Sato, T. Koyano, M. Mukai, and K. Kobayakawa, Abstract 109, p. 119, The Electrochemical Society Meeting Abstracts, Vol. 97-2, Paris, France, Aug 31-Sept 5, 1997.
156. M. M. Thackeray, M. H. Rossouw, R. J. Gummow, D. C. Liles, K. Pearce, A. De Kock, W. I. F. David, and S. Hull, *Electrochim. Acta*, **38,** 1259 (1993).
157. C. S. Johnson, M. F. Mansuetto, M. M. Thackeray, Y. Shao-Horn, and S. A. Hackney, *J. Electrochem. Soc.*, **144,** 2279 (1997).
158. L. Sanchez and J. L. Tirado, *J. Electrochem. Soc.*, **144,** 1939 (1997).
159. M. M. Thackeray, A. De Kock, and L. A. De Picciotto, *J. Power Sources*, **26,** 355 (1989).
160. H. Huang and P. G. Bruce, *J. Power Sources*, **54,** 52 (1995).
161. T. Ohzuku, A. Ueda, and M. Nagayama, *J. Electrochem. Soc.*, **140,** 1862 (1993).
162. R. J. Gummow and M. M. Thackeray, *J. Electrochem. Soc.*, **140,** 3365 (1993).
163. N. Imanishi, H. Kasiwagi, T. Ichikawa, Y. Takeda, and O. Yamamoto, *J. Electrochem. Soc.*, **140,** 315 (1993).
164. T. V. Nguyen and R. E. White, *Electrochim. Acta*, **38,** 935 (1993).
165. D. Fan and R. E. White, *J. Electrochem. Soc.*, **138,** 17 (1991).
166. D. Fan and R. E. White, *J. Electrochem. Soc.*, **138,** 2952 (1991).
167. D. M. Bernardi and M. K. Carpenter, *J. Electrochem. Soc.*, **142,** 2631 (1995).
168. J. Newman and W. Tiedemann, *J. Electrochem. Soc.*, 144, 3081 (1997).
169. J. S. Newman, *Electrochemical Systems*, 2nd ed., Prentice Hall, Englewood Cliffs, NJ (1991).
170. J. Newman and W. Tiedemann, *AIChE J.*, **21,** 25 (1975).
171. P. De. Vidts and R. E. White, *J. Electrochem. Soc.*, **144,** 1343 (1997).
172. W. Tiedemann and J. Newman, *J. Electrochem. Soc.*, 119, 186 (1972).
173. J. S. Dunning, D. N. Bennion, and J. Newman, *J. Electrochem. Soc.*, **120,** 906 (1973).
174. W. G. Sunu and D. N. Bennion, *J. Electrochem. Soc.*, 127, 2007 (1980).
175. K-C Tsaur and R. Pollard, *J. Electrochem. Soc.*, **133,** 2296 (1986).
176. D. Bernardi, *J. Electrochem. Soc.*, 137, 170 (1990).
177. O. Levenspiel, *Chemical Reaction Engineering*, 2nd ed., Wiley Eastern Limited, New York (1972).